1-1-2016

Functional Alterations in the Amygdala Following Traumatic Brain injury

Christopher Palmer
University of Pennsylvania, cpalmer487@gmail.com

Functional Alterations in the Amygdala Following Traumatic Brain injury

Abstract
Traumatic brain injury (TBI) afflicts approximately 3.8 million people each year, in the United States alone. In addition to the largely acute physical and cognitive symptoms of TBI, patients exhibit a heightened risk of developing persistent neuropsychological symptoms including anxiety, aggression, rage, depression/ anhedonia and apathy in the months to years after TBI. Despite the deleterious impact of these neuropsychological symptoms, very little is known of their neurological bases and there is currently no treatment targeting the underlying neuropathology giving rise to these symptoms. Employing a murine model of mild to moderate traumatic brain injury (mTBI), known as lateral fluid percussion injury (LFPI), we examined the effects mTBI on the physiology and function of the amygdala; a brain structure critical in processing emotional responses to sensory stimuli in humans. Behavioral experiments using a cued-fear conditioning paradigm, revealed significant deficits in the behavioral threat response of brain injured animals. We then utilized a combination of intracellular, extracellular, and voltage sensitive dye imaging (VSD) recording techniques to determine electrophysiological alterations in the amygdala following LFPI. These experiments revealed that LPFI causes a robust decrease in network excitability and circuit propagation strength in the basolateral and central amygdalae (BLA & CeA), without affecting the intrinsic excitability of BLA pyramidal neurons. Further experiments demonstrated that the injury-induced decrease in BLA network excitability is due in part to a decrease in glutamatergic excitation and preservation or augmentation of GABAergic inhibition; which increases the ratio inhibition to excitation in the amygdala of brain injured animals. This work demonstrates that mTBI has robust effects on amygdalar physiology that ultimately disrupt its normal function. The brain injury induced alterations in amygdalar function described herein, provide a potential neurological substrate for the neuropsychological symptoms suffered by TBI patients.

Degree Type
Dissertation

Degree Name
Doctor of Philosophy (PhD)

Graduate Group
Neuroscience

First Advisor
Akiva S. Cohen

Keywords
Amygdala, Behavioral threat response, Electrophysiology, LFPI, Traumatic Brain Injury, Voltage Sensitive Dye

Subject Categories
Neuroscience and Neurobiology

FUNCTIONAL ALTERATIONS IN THE AMYGDALA FOLLOWING TRAUMATIC BRAIN INJURY

Christopher P. Palmer

A DISSERTATION

in

Neuroscience

Presented to the Faculties of the University of Pennsylvania

in

Partial Fulfillment of the Requirements for the

Degree of Doctor of Philosophy

2016

Supervisor of Dissertation

_____

Akiva S. Cohen, PhD – Associate Professor of Anesthesiology and Critical Care

Graduate Group Chairperson

_____

Joshua I. Gold, PhD - Professor of Neuroscience

Dissertation Committee

Minghong Ma, PhD – Associate Professor of Neuroscience

Diego Contreras, MD, PhD – Professor of Neuroscience

David F. Meaney, PhD – Solomon R. Pollack Professor and Chair Bioengineering

Miranda M. Lim, MD, PhD – Assistant Professor of Medicine, PCCM; OHSU

FUNCTIONAL ALTERATIONS IN THE AMYGDALA FOLLOWING TRAUMATIC

BRAIN INJURY

ACKNOWLEDGMENT

It is often said, that the journey is the destination. In that sense, a PhD is not a proclamation of ones edification; it is an attestation to their dedication, a symbol of curiosity and resolve. While we all begin with these attributes, they can certainly be suppressed or fostered by the experiences and people in our lives, and so many people have fostered my curiosity and supported my dedication along the way. With more thanks owed and credit due than could possibly be expressed on this page, I want to begin simply by thanking everyone that has been a part of my journey so far. You all deserve and have my sincere gratitude, though I would be remiss to not mention a few people in particular.

To begin at the beginning, I would clearly not be the person I am today or a person at all, without the love and support of my parents and grandparents. Learning of or experiencing first hand your collective tenacity and determination throughout your lives, has made me eternally grateful for the opportunities you worked so hard to provide me. Seeing what you overcame and accomplished has shown me what self-confidence and resolve can realize, and shaped me into the stubborn ass I am today. Call it willpower if you like, but know that it came from you and that I am thankful, and better for it.

Doctors Peter West, Jean Hardwick, and Akiva Cohen, I blame each of you for making me a scientist! If all of you hadn't been such passionate, enlivening, and nurturing mentors I may of actually stood a chance of doing something else with my life. Joking aside, I would not have gotten here without each of your efforts. Peter, you started me down this path by letting a 19-year-old kid with no research background into your lab and onto your very nice patch-clamp rig; surely me dating the boss's daughter had

nothing to do with that! Alright, really all joking aside now, your excitement about neuroscience was utterly contagious and I could not ask for a better first mentor and friend. Jean, mama bear, that kind of says it all right? You treated everybody in your lab like family and you helped me accomplish something that I never imagined I was capable of, in getting into an Ivy League PhD program. Akiva, as you have told me many times, choosing a thesis lab is about more than the research, it's about finding an environment in which you can grow and succeed. Your willingness to let me follow my interests and instincts, all the while battling my pessimism with your upbeat attitude, has truly helped me to grow as a scientist and a person. When I look back on all the excited conversations about new data, occasional head butting and the many laughs that we shared, I know I made the right choice of mentor. You will always have my respect, admiration, and thanks. To all the members of the Cohen lab, especially Dr. Brian Johnson, thank you for making it a great place to work and for all that you taught me. Thank you all.

A monumental thank you to friends and family who supported and kept me sane over the past 5 years. Russell Port, Colin Smith, and the whole UPenn NGG crew, whether we were treating our bodies as a temple at the gym, or like an amusement park at the pub, thank you guys for always being there with a helping hand or one holding a fresh beer. I'm lucky to have each of you as a friend. Speaking of luck, you don't get to choose your family, or your in-laws, but I lucked out on both. Roche family, I don't know the words to describe how happy and fortunate your loving acceptance of me as a brother and a son have made me feel; thank you guys for everything.

Finally, last but certainly not least, the aforementioned boss's daughter, my beautiful wife Meghan. In many ways meeting you is what started me on this journey,

and you have been by my side the whole way, never doubting or discouraging, always urging onward, always dreaming. Your dreams are more precious to me than any embroidered cloth of heaven, yet I know I do not often tread lightly. Thank you so much for all that you do, put up with, and for loving me through thick and thin (literally); I couldn't have done this without you. As we embark on a new journey together, we face many uncertainties. Where will we go? What route will we take there? And I understand that my carefree embrace of this uncertainty vexes you. So allow me to explain, I may not know where I'm going or how I'll get there, but I know that I'm going with you and our not so little dog too. Whether we don't move an inch or end up in Oz, I can't wait, because I know the only thing that really matters will be by my side, as you have been since the day I met you.

ABSTRACT

FUNCTIONAL ALTERATIONS IN THE AMYGDALA FOLLOWING TRAUMATIC BRAIN INJURY

Christopher P. Palmer

Akiva S. Cohen, PhD

Traumatic brain injury (TBI) afflicts approximately 3.8 million people each year, in the United States alone. In addition to the largely acute physical and cognitive symptoms of TBI, patients exhibit a heightened risk of developing persistent neuropsychological symptoms including anxiety, aggression, rage, depression/anhedonia and apathy in the months to years after TBI. Despite the deleterious impact of these neuropsychological symptoms, very little is known of their neurological bases and there is currently no treatment targeting the underlying neuropathology giving rise to these symptoms. Employing a murine model of mild to moderate traumatic brain injury (mTBI), known as lateral fluid percussion injury (LFPI), we examined the effects mTBI on the physiology and function of the amygdala; a brain structure critical in processing emotional responses to sensory stimuli in humans. Behavioral experiments using a cued-fear conditioning paradigm, revealed significant deficits in the behavioral threat response of brain injured animals. We then utilized a combination of intracellular, extracellular, and voltage sensitive dye imaging (VSD) recording techniques to determine electrophysiological alterations in the amygdala following LFPI. These experiments revealed that LPFI causes a robust decrease in network excitability and circuit propagation strength in the basolateral and central amygdalae (BLA & CeA), without

affecting the intrinsic excitability of BLA pyramidal neurons. Further experiments demonstrated that the injury-induced decrease in BLA network excitability is due in part to a decrease in glutamatergic excitation and preservation or augmentation of GABAergic inhibition; which increases the ratio inhibition to excitation in the amygdala of brain injured animals. This work demonstrates that mTBI has robust effects on amygdalar physiology that ultimately disrupt its normal function. The brain injury induced alterations in amygdalar function described herein, provide a potential neurological substrate for the neuropsychological symptoms suffered by TBI patients.

TABLE OF CONTENTS

ACKNOWLEDGMENT ..... **III**

ABSTRACT ..... **VI**

LIST OF TABLES ..... **IX**

LIST OF FIGURES ..... **X**

INTRODUCTION **1**

CHAPTER 2 ..... **17**

HIGHLIGHTS: 18

ABSTRACT: 19

INTRODUCTION: 20

MATERIALS AND METHODS: 22

RESULTS: 33

DISCUSSION: 42

ACKNOWLEDGMENTS: 48

TABLE LEGENDS: 49

FIGURE LEGENDS: 51

TABLES: 61

FIGURES: 63

CHAPTER 3 ..... **74**

ABSTRACT: 75

INTRODUCTION: 77

MATERIALS AND METHODS: 80

RESULTS: 86

DISCUSSION: 91

FIGURE LEGENDS: 96

FIGURES: 105

CONCLUSIONS AND FUTURE DIRECTIONS **114**

BIBLIOGRAPHY **123**

LIST OF TABLES

Chapter 1: Introduction

Table 1: Aggression, anxiety, depression, and fear like behaviors in animal models of traumatic brain injury: a review of publish findings……16

Chapter 2: Diminished amygdala activation and behavioral threat response following traumatic brain injury

Table 1: Group median peak ΔF/F values, 95% confidence intervals and *P* values for all peaks at all stimulation intensities ...……61

Table S1: Group median peak ΔF/F values and *P* values for all amygdala regions in the presence of APV+CNQX or pre and post CGP55845…….……62

LIST OF FIGURES

Chapter 2: Diminished amygdala activation and behavioral threat response following traumatic brain injury

Figure 1: LFPI decreases freezing in a cued fear conditioning paradigm…….....63

Figure 2: LFPI decreases lateral amygdala evoked basolateral amygdala fEPSPs……...64

Figure 3: Amygdala VSD imaging recording set-up and representative movie frames…65

Figure 4: VSD average raster plots and multi segment regional averages showing LFPI-induced alterations in amygdala activation……..…….....66

Figure 5: Amygdala VSD peak maps and regional activation ratios showing decreased propagation in amygdala circuit following LFPI……...67

Figure 6: BLA Pyramidal neuron intrinsic excitability…….68

Supplemental Figure 1: APV and CNQX isolated fEPSP fiber volleys……69

Supplemental Figure 2: APV and CNQX……...……...70

Supplemental Figure 3: CGP 55845……..71

Supplemental Video 1…….……...72

Supplemental Video 2…….……...72

Chapter 3: Preliminary findings on the mechanism of traumatic brain injury induced decreased network excitability of the basolateral amygdala

Figure 1: sEPSCs are blocked by bath application of APV and CNQX……105

Figure 2: sEPSC frequency onto BLA pyramidal neurons is decreased following LFPI…….106

Figure 3: Lateral amygdala stimulation eEPSCs onto BLA pyramidal neurons are decreased following LFPI……107

Figure 4: Lateral amygdala stimulation eEPSCs are blocked by bath application of APV and CNQX……...108

Figure 5: Lateral amygdala stimulation eIPSCs onto BLA pyramidal neurons are unaffected by LFPI……..109

Figure 6: Lateral amygdala stimulation eIPSCs are blocked by bath application of bicuculline methiodide (BMI) ……110

Figure 7: Intra cell lateral amygdala stimulation eIPSC/eEPSC ratio is significantly augmented following LFPI……..111

Figure 8: Lateral amygdala stimulation eIPSCs are largely abolished by application of APV and CXQX……..112

Figure 9: Simplified basolateral amygdala circuit schematic…….…….113

INTRODUCTION

Traumatic brain injury (TBI) is a growing national and global epidemic with far reaching impacts on patients, families, and economies. In the United States alone an estimated 1.7-3.8 million traumatic brain injuries occur each year; a number that has steadily risen over the past two decades (Langlois et al., 2006; Rutland-Brown et al., 2006; Faul and Coronado, 2015). Incidence of TBI is believed to be even higher in developing countries, a recent study estimated that by the year 2050 there will be as many as 14 million new cases of TBI in Africa each year (Wong et al., 2015). TBI occurs most frequently in children (0-4 years old), the elderly (75+ years old), and adolescents/young adults (15-25 years old); commonly resulting from falls, motor vehicle accidents, sports, and interpersonal violence (Langlois et al., 2006; Faul and Coronado, 2015). Severe TBI has a substantial mortality rate, and is a leading cause of death in children and young adults. However, the most common form of TBI, mild traumatic brain injury (mTBI) (i.e. concussion), which comprise approximately 80% of brain injuries, is not typically life threatening. The historical increase in incidence of TBI mentioned above has also coincided with a decrease in overall mortality rate, likely due to advances in treatment and awareness of TBI. The high prevalence of mild injuries combined with opposing trends in incidence and mortality, and the fact that most of these injuries are occurring in children and young adults, all point towards a growing population of young TBI survivors at risk of developing or currently suffering TBI related disability.

Patients who sustain even mild TBI commonly develop some combination of post-traumatic symptoms in the days to weeks following injury. Post-traumatic symptoms can be broadly segmented into three main categories: physical, cognitive, and emotional symptoms. Common physical symptoms include headache, dizziness, photophobia, nausea, vomiting, insomnia and fatigue. Cognitive deficits in working memory, executive function and focus often manifest as confusion, difficulty concentrating, and a feeling of fogginess or mental lethargy (Alves et al., 1993; Johansson et al., 2009; Benedictus et al., 2010; D et al., 2011; Blume and Hawash, 2012; Slovarp et al., 2012). Emotional or neuropsychological symptoms are the most variable and seem to be somewhat bi-directional in nature, with symptoms that involve either a heightened or suppressed emotional state. These symptoms include anxiety, agoraphobia, aggression, irritability, rage, poor impulse control, depression, apathy, and anhedonia (McAllister, 1992; Jorge et al., 2004; Rao et al., 2009; Riggio, 2010; Blennow et al., 2012; Scholten et al., 2016).

The physical and cognitive symptoms suffered by mTBI patients typically present acutely after injury, and in the majority of patients spontaneously resolve within days to weeks after injury. However, approximately 10-15% of patients exhibit persistent physical or cognitive symptoms at one year post injury (McAllister, 1992; D et al., 2011; Faul and Coronado, 2015). Unlike the physical and cognitive symptoms that manifest and largely resolve acutely after TBI, neuropsychological symptoms often manifest months or years later and never fully resolve (Jorge et al., 2004; Scholten et al., 2016). The sub-acute, persistent nature of these neuropsychological symptoms likely makes them disproportionately responsible for the long-term negative outcomes seen in TBI patients.

TBI and the symptoms associated with it have a considerable deleterious impact on the lives of survivors and our society as a whole. Undoubtedly due to the myriad of aforementioned symptoms, TBI survivors often have trouble maintaining relationships and returning to full-time employment; with only about 72% of people who suffered even just mTBI, returning to full-time employment by 1 year after injury (Benedictus et al., 2010; Malkesman et al., 2013). With that perspective, it's not hard to imagine how the neuropsychological symptoms, social isolation, and inability to resume employment, all compound in these patients to promote very negative potential outcomes. And indeed, TBI survivors do have an increased likelihood of substance abuse, incarceration, suicidality, and death (McAllister, 1992; Langlois et al., 2006). The economic impact is also substantial, with the direct and indirect costs of TBI totaling upwards of $60 billion a year in the Unites States alone (Finkelstein et al., 2006; Faul and Coronado, 2015). Yet despite the pervasive, destructive and expensive nature of TBI, there is currently no effective treatment targeting the underlying pathology of TBI. Current treatments are limited to physical and cognitive rest, palliative treatment of symptoms, and behavioral therapies, all of which are met with limited success.

In order to develop successful future therapeutics for the treatment of cognitive and neuropsychological symptoms of TBI, we first need to understand the physiological consequences of TBI that underlie these symptoms. Studies of human TBI patients assessing higher order brain function and connectivity using resting state functional magnetic resonance imaging, diffusion tensor imaging, and event related potential recordings, have identified network level dysfunction and alterations in regional

activation of the human brain following TBI (Duncan et al., 2003; McAllister et al., 2006; Dockree and Robertson, 2011; Mayer et al., 2011; Blennow et al., 2012; Johnson et al., 2012; Sharp et al., 2014; Han et al., 2015). Further, some of these studies have linked functional alterations of certain brain regions to a corresponding cognitive or neuropsychological symptom; such as, altered amygdala connectivity corresponding with depression, or prefrontal hypoactivation with working memory deficits (Sánchez-Carrión et al., 2008; Han et al., 2015). Overall, these studies and others like them identify TBI as an electrophysiological disorder that produces network or circuit level dysfunction associated with cognitive and neuropsychological disorders. Therefore, in order to study and characterize the neurophysiological mechanisms underlying network dysfunction of susceptible human brain regions, many researchers have turned to various animal models of TBI that allow in depth characterization of synaptic and circuit function following TBI.

To date, the majority of both human and animal research performed in the field of TBI has focused on the cognitive symptoms and brain regions important in learning and memory. In particular the hippocampus, a brain region integral in learning and memory, has been heavily studied in animal models of TBI. This work has identified regional shifts in the balance of excitation and inhibition (E/I balance) associated with deficits in spatial memory following TBI. Specifically, TBI causes an increase in network excitability of the dentate gyrus and an opposing decrease in excitability and output of area CA1 of the hippocampus (Santhakumar et al., 2002; Witgen et al., 2005; Johnson et al., 2014). Further, pharmacological restoration of hippocampal excitability following

TBI ameliorates behavioral deficits in spatial memory (Cole et al., 2010); suggesting, that the disruption of E/I balance in the hippocampus underlies the spatial memory deficit. Continued investigations into the mechanism of the injury-induced shifts in hippocampal E/I balance have identified cell type specific effects contributing to regional changes in network excitability. For example, one study found that brain injury induces hyperexcitability of semilunar granule cells within the dentate gyrus, which likely contribute to the overall increase in excitability and throughput of the dentate following TBI (Gupta et al., 2012). Additionally, work from our laboratory has shown that augmented inhibition from CCK+ interneurons contributes to the decrease in network excitability and suppression of action potential generation in pyramidal neurons of region CA1 following TBI (Johnson et al., 2014). Overall, this work suggests that certain cell types in discrete brain regions are uniquely susceptible to damage from brain injury and can create circuit level dysfunction.

While cognitive deficits and memory loss are obviously important consequences of TBI that need to be understood and therapeutically addressed, they represent only a few of the many debilitating symptoms suffered by TBI patients. Furthermore, unlike cognitive deficits, which are transient in the vast majority of patients, the proportion of TBI patients suffering emotional or neuropsychological symptoms actually increases over time since injury. Thus, not only are patients developing neuropsychological symptoms, but these symptoms often persist for years after onset (Scholten et al., 2016). Emotional or neuropsychological symptoms account for a large proportion of TBI related disability, especially in the long term and yet have received a disproportionately small amount of

research attention. As such, a current focus of TBI research is to utilize the results of experiments examining the physiological underpinnings of cognitive deficits following TBI, to help design and execute new experiments toward understanding the physiological alterations underlying the acquisition or expression of emotional symptoms following TBI. To do this, we can build upon 1) human research studies that have tentatively identified brain regions involved in these symptoms, and 2) the limited body of animal work performed on this topic to date.

Based on the known function of brain regions and the complement of neuropsychological symptoms common in TBI patients, we can readily hypothesize that some part of the fronto-limbic system, important in generating human emotion (Ledoux, 2000; Cardinal et al., 2002; LeDoux, 2012), is commonly damaged or altered by TBI. The amygdala, a limbic structure critical in the conscious and autonomic response to emotional stimuli, is commonly hypothesized to be damaged by TBI and responsible for post-injury neuropsychological symptoms. The amygdala's high degree of efferent and afferent connections to memory, decision making, reward, autonomic and sensory regions of the brain do make it uniquely well-suited to underlie the widespread and varied effects on emotion (Ledoux, 2000; Sah et al., 2003), seen in TBI patients. Affirmatively, functional alterations in the amygdala have been directly linked to most of the neuropsychological symptoms seen in TBI patients, although the majority of these studies were performed in patient cohorts not limited to TBI (Ledoux, 2000; Cardinal et al., 2002; Phelps and LeDoux, 2005; Liao et al., 2012; Duvarci and Pare, 2014). Furthermore, brain injury-induced damage to the amygdala could represent a potential

substrate for the comorbidity of TBI and post-traumatic stress disorder (PTSD) (Riggio, 2010; Depue et al., 2014), a known disorder of the amygdala. Finally, perhaps the strongest support of the amygdala hypothesis for neuropsychological symptoms comes from two recent studies linking changes in human amygdalar connectivity or diffusivity to the expression of depression or anxiety disorders respectively in TBI patients (Juranek et al., 2011; Han et al., 2015). Due to these indications and the wealth of primary research characterizing amygdala physiology and function, the amygdala has become a primary focus of animal research on the neuropsychological symptoms of TBI.

Most of the animal research on the neuropsychological symptoms of TBI has focused on modeling and assessing animal behavioral correlates to the most common human neuropsychological symptoms (anxiety and depression), in rodent models of TBI. Interestingly, across the dozens of animal studies that have been performed, no consensus on the direction or presence of these symptoms was ever reached. Studies on anxiety like behaviors in rodent models of TBI have shown contradictory results using a variety of behavioral paradigms to assess anxiety. Even using the same behavioral paradigm some research groups found consistent increases in anxiety like behavior, others consistent decreases and yet others no change, following TBI. When assessing depression like behaviors in brain injured animals, there was again inconsistency within the literature, with some reporting the development of symptoms and others not (**Table 1**, see (Malkesman et al., 2013) for a detailed review of this literature). While this contradiction may initially seem troublesome, I propose that these results actually well replicate what is seen in the human TBI patient population. When interpreting the results of these studies

we must consider two important factors; first, human TBI is an extremely heterogeneous injury that can result in an array of neuropsychological symptoms, or none at all. Second, rodent brain injury models were designed to create consistent, reproducible injuries of the same nature; but no two injury models create the exact same injury, based on the parameters and type of injury model used. Thus, individual animal models of TBI inherently lack injury heterogeneity, but when we combine studies using various injury models and post injury time points, we're actually viewing the results of a heterogeneous injury; which is a much better representation of human TBI as a whole. If we consider the summed findings on anxiety and depression like behaviors across all animal studies, it actually represents the human TBI population relatively well; where only some individuals develop neuropsychological symptoms and the symptom or symptoms they develop can be extremely varied. Hence, it is plausible that different animal brain injury protocols (reviewed in (Xiong et al., 2013)) are simply modeling different human TBI patient populations, rather than producing contradictory findings.

Given the variability of amygdala-associated behavioral symptoms following experimental TBI, is there similar variability in amygdala physiology following TBI? Physiological investigations of the amygdala in animal models of TBI are still extremely limited. Two studies, one assessing GAD-67 and NR1 protein levels in the basolateral amygdala (BLA) and the other spontaneous synaptic inhibition in the BLA, suggest an increase in amygdalar excitability following TBI (Reger et al., 2012; Almeida-Suhett et al., 2014). Published findings presented later in this thesis demonstrate a decrease in amygdalar excitability and circuit strength following TBI (Palmer et al., 2016). Yet,

another study shows opposing shifts in amygdalar excitability dependent upon the level of pre injury stress to which the animal was subjected, adding another level of complexity to the interpretation of these studies and the development of neuropsychological symptoms in human TBI patients (Klein et al., 2015). While these four physiological studies hardly represent the quantity or diversity of the behavioral studies mentioned above, thus far they follow a similar pattern of variability.

The goal of the experiments presented in this thesis is to expand our limited understanding of brain injury-induced alterations in amygdala physiology and amygdala-dependent behaviors. As it is clear that the injury model and parameters used will likely affect the nature of the results of these experiments; we chose a well-established, current murine model of mild to moderate traumatic brain injury, known as lateral fluid percussion injury (LFPI). Murine LFPI has been widely used since its development in the 1980's and remains one of the most commonly used animal models of TBI (Thompson et al., 2005; Xiong et al., 2013). LFPI creates a reproducible, non-penetrating local and diffuse brain injury that mimics many aspects of human TBI pathology and symptomatology (Carbonell et al., 1998; Thompson et al., 2005; Xiong et al., 2013). Using this model not only allows us to compare our findings to previous results from our laboratory, but also makes these studies relevant to the many research groups that use a similar injury model.

To begin our investigation of functional alterations in the amygdala following LFPI, we first sought to identify injury-induced alterations in an amygdala-dependent

behavior, as not all injury paradigms produce behavioral deficits in amygdala-associated behaviors. Although there are many different behavioral assays for amygdala-associated behaviors such as anxiety and depression, the animal behavior assessed in many of these paradigms represents the intersection of multiple motivations. The elevated plus maze for instance, may involve fear of open spaces along with a drive to explore novel spaces; such that a change in the amount of time an animal spends in an open arm could be due to a change in either or both motivations. The complexity inherent in generating an animal behavior, in a behavioral paradigm assessing animal behavioral correlates to human neuropsychological symptoms, makes it difficult to correlate an alteration in these animal behaviors directly to alterations in amygdalar physiology. As such, we chose to examine a more basic and instinctual response to sensory stimuli by assessing behavioral threat response in a cued fear conditioning paradigm. The behavioral threat response (aka. cued fear) paradigm allows for a more straightforward assessment of a specifically amygdala-dependent behavior. The physiological mechanisms underlying this behavior are extremely well characterized. It is known that acquisition and expression of a threat response, in this instance freezing, in response to a light and/or tone cue paired with an aversive stimuli, is dependent upon physiological processes within the basolateral and central amygdalae (Phillips and Ledoux, 1992; Dębiec et al., 2010; Tronson et al., 2012; Duvarci and Pare, 2014). Accordingly, alterations in a behavioral threat response correlate to physiological alterations in the amygdala much more reliably than alterations in anxiety and depression like behaviors. Another advantage of cued fear conditioning, is that we are explicitly removing the hippocampal based spatial learning and memory component, which we know is impaired by TBI. Removal of spatial cues is accomplished

by altering the context between the training and testing phases of the cued fear conditioning paradigm, thus negating any spatial associations to the aversive stimuli (Phillips and Ledoux, 1992; Ledoux, 2000). Fear potential startle (FPS) is another behavior that could have been assessed as a measure of amygdala function following TBI, as it involves a similar set of neural circuits as behavioral threat response.

Our experiments revealed a significant decrease in the behavioral threat response of brain injured animals 7 days post LFPI; demonstrating that our brain injury model causes deficits in an amygdala dependent behavior. It is of note that this acute post-injury time point is not typically correlated with the sub acute expression of human neuropsychological symptoms following TBI. The purpose of assessing amygdala function acutely was to characterize the initial effects of injury that may ultimately underlie or contribute to the development of neuropsychological symptoms in the months to years following traumatic brain injury.

Next, we characterized amygdalar physiology by stimulating the primary input-receiving region of the amygdala, the lateral amygdala (LA), while recording the response evoked throughout the amygdala in brain slices prepared from sham and brain-injured animals. More precisely, we performed a series of extracellular recordings together with voltage sensitive dye imaging (VSD) to assess network excitability and circuit strength in the basolateral and central amygdalae (BLA & CeA) following LFPI. As a diminished behavioral threat response is typically associated with a decrease in network excitability of the BLA and CeA, we hypothesized a decrease in activation of the

BLA & CeA following LFPI. It is important to note, that this association between behavior and BLA physiology is based on an oversimplified view of neural circuitry within and afferents onto, the BLA; thus that an unexpected or opposing physiological result would not contradict the known circuitry of the BLA. Likewise, the intranuclear circuit complexity of the CeA is commonly downplayed when linking physiology and behavior, though the medial portion of the CeA does contain projection neurons that directly influence brain regions mediating the instinctual response to threat, assessed in this behavioral paradigm (Sah et al., 2003; Ehrlich et al., 2009; Duvarci and Pare, 2014). While it is reasonable to base hypotheses on gross amygdala circuitry and typical physiological correlates to behavior, the author cautions against overconfidence or overinterpretation of experimental results based on a simplified amygdalar circuit. Data from our experiments did indeed demonstrate a significant decrease in activation of both the BLA and CeA, and a weakening of inter-nuclear amygdala circuit strength following LFPI.

After identifying injury-induced alterations in the amygdala circuit associated with deficits in amygdala dependent behaviors, we then sought to determine the cellular mechanisms underlying the decrease in amygdalar excitability and function. To that end, we examined amygdalar excitability and synaptic function, by performing a series of whole-cell recordings of BLA pyramidal neurons in brain slices from sham and LFPI animals. Pyramidal neurons are the principal excitatory cell type and comprise approximately 80% of the neurons within the BLA. These neurons integrate inputs from multiple brain regions including the LA and internal/external capsules, which carry

sensory information to the BLA. Pyramidal neurons in turn provide the primary output of the BLA by projecting to downstream amygdalar nuclei (i.e. CeA) and also other brain regions including the prefrontal cortex, striatum, nucleus accumbens, and hippocampus (Sah et al., 2003; Duvarci and Pare, 2014).

Based on data from our previous experiments, two plausible causes for the injury-induced decrease in amygdala activation include an alteration of the intrinsic properties of excitatory cells within the BLA, an alteration of inputs onto those cells, or both. Thus to begin, we performed a series of whole-cell current-clamp recordings to assess the membrane properties and intrinsic excitability of BLA pyramidal neurons. These experiments demonstrated that LFPI has no effect on any measure of intrinsic excitability of BLA pyramidal neurons. After ruling out the possibility that changes in intrinsic excitability of BLA pyramidal neurons contribute to the decrease in amygdala activation following LFPI, we next investigated synaptic inputs onto these neurons as a potential source of the decrease in amygdalar excitability.

Utilizing whole-cell voltage-clamp, we began the examination of synaptic function in the BLA by recording spontaneous excitatory post synaptic currents (sEPSCs) onto BLA pyramidal neurons. Data from these experiments demonstrated a decrease in spontaneous excitatory (glutamatergic) neurotransmission or excitatory tone in the BLA following LFPI. To further characterize synaptic function and directly compare glutamatergic excitation to GABAergic inhibition within the same BLA pyramidal neurons; we recorded LA stimulation evoked glutamatergic excitatory post synaptic

currents and GABAergic inhibitory post synaptic currents (eEPSCs & eIPSCs), in neurons from brain slices from sham and LFPI animals. Overall, the investigations of synaptic function in the BLA following LFPI revealed alterations in excitation and inhibition that increased the ratio of inhibition to excitation within the BLA, and likely underlie the decrease in activation of the amygdala following LFPI.

To summarize, LFPI induces a decrease in glutamatergic excitatory drive, coupled with a preservation or augmentation of GABAergic inhibition, resulting in a decrease in amygdala excitability coinciding with a decreased behavioral response to threatening stimuli. This work indicates that mTBI can have robust effects on amygdalar physiology that ultimately disrupt its normal function and alter behavioral outputs. Beyond expanding our understanding of circuit level effects of mTBI in the amygdala, this works provides a paradigm in which to test future therapeutics targeted at mitigating or ameliorating mTBI-induced amygdala dysfunction, which likely contributes to the development of neuropsychological symptoms.

Table Legends

Table 1: Aggression, anxiety, depression, and fear like behaviors in animal models of traumatic brain injury: a review of published findings. Column 1 contains the behavioral task/s assessed followed by the human neuropsychological symptom this animal behavior is thought to correlate to. Columns 2-4 reference published studies using animal models of TBI that are segregated into columns of increase, decrease, or no change in the behavioral output measured by the given paradigm, based on the studies findings. References cited in table 1: (Milman et al., 2005; Cutler et al., 2006; Taylor et al., 2006; Tweedie et al., 2007; Wagner et al., 2007; Jones et al., 2008; Vučković et al., 2008; Pandey et al., 2009; Schwarzbold et al., 2010; Ajao et al., 2012; Kimbler et al., 2012; Reger et al., 2012; Semple et al., 2012; Shultz et al., 2012; Siopi et al., 2012; Washington et al., 2012; Yu et al., 2012; Budinich et al., 2013; Almeida-Suhett et al., 2014; Chen et al., 2014; Palmer et al., 2016).

Tables

Table 1

Behavioral Tests:	Decreased:	No Change:	Increased:
Elevated-plus/Zero maze (Anxiety)	Pandey et al. Washington et al.	Cutler et al. Siopi et al.	Shultz et al. Schwarzbold et al. Ajao et al.
Forced swim/Tail suspension (Depression)	Kimbler et al.	Jones et al. Schwarzbold et al. Vuckovic et al.	Milman et al. Taylor et al. Tweedie et al. Washington et al.
Open field (Anxiety/Depression)		Jones et al. Wagner et al.	Almedia-Suhett et al. Yu et al. Budinich et al.
Resident-intruder (Aggression)			Semple et al.
Cued-fear conditioning (Fear)	Palmer et al.	Chen et al.	Reger et al.

CHAPTER 2

Diminished amygdala activation and behavioral threat response following traumatic brain injury

Christopher P. Palmer [a], Hannah E. Metheny [b], Jaclynn A. Elkind [b], Akiva S. Cohen [b,c]

[a] Neuroscience Graduate Group and [c] Critical Care Medicine, Department of Anesthesiology, Perelman School of Medicine, University of Pennsylvania: 3451 Walnut Street, Philadelphia, PA 19104

[b] Critical Care Medicine, Department of Anesthesiology, The Children's Hospital of Philadelphia: 3401 Civic Center Blvd, Philadelphia, PA 1910

Originally published as: Palmer, C. P., Metheny, H. E., Elkind, J. A., & Cohen, A. S. (2016). Diminished amygdala activation and behavioral threat response following traumatic brain injury. Experimental Neurology, 277, 215–226. http://doi.org/10.1016/j.expneurol.2016.01.004

Highlights:

- Brain injury (LFPI) caused a decrease in amygdala-dependent cued threat response

- LFPI induced a decrease in network excitability of the basolateral amygdala

- Strength of internuclear amygdala projections was significantly weakened by LFPI

- LFPI had no effect on the intrinsic excitability of amygdala principal neurons

Abstract:

Each year, approximately 3.8 million people suffer mild to moderate traumatic brain injuries (mTBI) that result in an array of neuropsychological symptoms and disorders. Despite these alarming statistics, the neurological bases of these persistent, debilitating neuropsychological symptoms are currently poorly understood. In this study we examined the effects of mTBI on the amygdala, a brain structure known to be critically involved in the processing of emotional stimuli. Seven days after lateral fluid percussion injury (LFPI), mice underwent a series of physiological and behavioral experiments to assess amygdala function. Brain injured mice exhibited a decreased threat response in a cued fear conditioning paradigm, congruent with a decrease in amygdala excitability determined with basolateral amygdala (BLA) field excitatory post synaptic potentials together with voltage sensitive dye imaging (VSD). Furthermore, beyond exposing a general decrease in the excitability of the primary input of the amygdala, the lateral amygdala (LA), VSD also revealed a decrease in the relative strength or activation of internuclear amygdala circuit projections after LFPI. Thus, not only does activation of the LA require increased stimulation, but the proportion of this activation that is propagated to the primary output of the amygdala, the central amygdala, is also diminished following LFPI. Intracellular recordings revealed no changes in the intrinsic properties of BLA pyramidal neurons after LFPI. This data suggests that mild to moderate TBI has prominent effects on amygdala function and provides a potential neurological substrate for many of the neuropsychological symptoms suffered by TBI patients.

Introduction:

Traumatic brain injury (TBI) afflicts approximately 3.8 million people annually in the United States alone, with at least 5.3 million or 2% of the US population suffering persistent TBI-related disability (Langlois et al., 2006; Rutland-Brown et al., 2006; Faul and Coronado, 2015). Even mild to moderate traumatic brain injury (mTBI i.e. concussion), the most common form of TBI, results in debilitating symptoms and cognitive dysfunction. Whereas much of the animal research performed on mTBI has focused on cognition and memory (Xiong et al., 2013), cognitive deficits and memory impairment represent only a few of the debilitating neuropsychological symptoms suffered by mTBI patients. Many other prominent symptoms including, anxiety, aggression/irritability/rage, depression/anhedonia, apathy, and poor impulse control indicate emotional destabilization following mTBI (Jorge et al., 2004; Bazarian et al., 2009; Rao et al., 2009; Riggio, 2010; Malkesman et al., 2013).

Functional alterations in the amygdala, a brain region critically involved in the conscious and autonomic response to emotional stimuli, are associated with many if not all of the aforementioned symptoms (Ledoux, 2000; Cardinal et al., 2002; Phelps and LeDoux, 2005; Duvarci and Pare, 2014). Furthermore, if concussion induces acute physiological alterations in the amygdala, this could represent a potential substrate for the substantial comorbidity of traumatic brain injury and post-traumatic stress disorder (PTSD) (Riggio, 2010). While a limited number of human studies linking changes in amygdala size and diffusivity (diffusion tensor imaging) to TBI have been performed (Juranek et al., 2011; Depue et al., 2014), there exists a dearth of studies concerning

amygdala physiology and dysfunction following mTBI. Understanding the effects of mTBI on amygdala function is critical for the development of therapeutic interventions to treat mild to moderate TBI and further our understanding of how mTBI relates to PTSD.

Using a well-established mouse model of mTBI, lateral fluid percussion injury (LFPI) (Thompson et al., 2005; Xiong et al., 2013), physiological and behavioral experiments were performed to determine the effects of mTBI on amygdala function. As the amygdala is a critical component of threat response (freezing behavior), our studies began by testing animals for the acquisition and expression of threat response in a cued fear conditioning paradigm. Next, extracellular recording together with voltage sensitive dye (VSD) imaging was conducted to examine network activity and circuit function across multiple amygdala sub-regions, in brain slices from sham and brain-injured animals. VSD imaging allowed us to determine how brain injury effects local responses in the stimulated amygdala sub-regions, and further determine how this activation propagated to other amygdala nuclei; thus revealing potential changes in amygdala circuit dynamics. Finally, intracellular recordings were performed to assess intrinsic properties of amygdala neurons following LFPI. Through the combined use of physiological and behavioral techniques we have identified circuit level dysfunction in the amygdala corresponding to deficits in threat response in brain-injured animals.

Materials and Methods:

Animals

All experiments were performed on 7 to 12 week-old, male C57BL/J6 mice (The Jackson Laboratory). All animals were group housed with free access to food and water. All procedures were performed in accordance with the guidelines published in the National Institutes of Health (NIH) Guide for the Care and Use of Laboratory Animals and approved by the Children's Hospital of Philadelphia Institutional Animal Care and Use Committee. Behavioral and physiological experiments were performed on separate cohorts of animals.

Lateral Fluid Percussion Injury

LFPI is a well-established model of mild to moderate traumatic brain injury that mimics many aspects of human TBI pathology and symptomatology (Carbonell et al., 1998; Thompson et al., 2005; Xiong et al., 2013). Animals were randomly assigned into three groups; Naïve animals that received no surgery or injury, but were treated otherwise identically; LFPI (surgery+injury); or sham (surgery only). Surgery and injury were performed on consecutive days, for full details see (Witgen et al., 2005; Cole et al., 2010). Briefly, on day one mice were anesthetized with a combination of ketamine (100 mg/kg) and xylazine (10 mg/kg) and placed in a stereotaxic frame (Stoelting). A 3 mm outer diameter trephine was then used to perform a craniectomy of the right parietal bone lateral of the sagittal suture between lambda and bregma, without disrupting the intact dura. A Luer-loc needle hub (3 mm inner diameter) was secured to the skull surrounding

the craniectomy with adhesive and dental cement. The needle hub was filled with sterile saline solution and sealed overnight. On the following day, LFPI animals were anesthetized with isoflurane and connected to the LFPI device (Department of Biomedical Engineering, Virginia Commonwealth University, Richmond, VA). The LFPI device was then triggered, delivering a 10-15 ms fluid pulse (peak pressure 1.5-1.8 atm) onto the intact dura of the brain to generate a mild to moderate TBI. The needle hub was removed and the incision sutured. Any animals with injuries resulting in dural breach or herniation were excluded from the study. Sham animals underwent an identical procedure without receiving the fluid pulse injury. Since no significant differences between sham and naïve animals were evident, these two groups were pooled for analysis and referred to as the sham group.

Cued Fear Conditioning

It is well established that acquisition and expression of a threat response, that is freezing, to a light and/or tone cue, paired with an aversive stimuli, is dependent upon physiological processes within the basolateral and central amygdalae (Phillips and Ledoux, 1992; Dębiec et al., 2010; Tronson et al., 2012; Duvarci and Pare, 2014). Fear conditioning paradigms pair an emotionally neutral stimulus or context (conditioned stimulus or CS) with an aversive stimulus (unconditioned stimulus or US), leading to the expression of a threat response to presentation of the neutral CS alone. As noted, both the context and cue become predictive of the US and elicit a threat response. For these experiments the context was altered between training (context A) and testing (context B)

to isolate the light/tone (CS) cued response from the hippocampal dependent contextual response.

The cued fear conditioning paradigm used in this study was modified from experiments described in (Newton et al., 2004; Wolff et al., 2014). The CS consisted of simultaneous auditory (75dB, white noise, 20s) and light stimuli (yellow light pulses, 20s, flickering at 4 Hz) generated by built in audio and light stimuli generators (Med Associates, St. Albans, VT, USA). The US consisted of a footshock (1.05mA, 1.5s) delivered through the metal grid floor. During CS-US pairings, the US was delivered immediately following the cessation of the CS. All behavioral experiments were performed in an isolated behavioral suite under low light.

On days 4 and 5 after injury or sham operation, each animal was handled for 3 min by the experimenter. On day 6 animals underwent fear conditioning training in context A, a rectangular conditioning chamber (21.6 cm x 17.8 cm x 12.7 cm) with Plexiglas and metal walls, and a metal grid floor (Med Associates, St. Albans, VT, USA). Animals were allowed to freely explore the chamber for 1 min before experiencing 3 CS-US pairings (15s - 105s interstimulus interval, mean 60s). The mean of the first and second interstimulius intervals (ISI) was consistently 60s, with the actual duration of ISI 1 vs ISI 2 assigned pseudo-randomly within a group, but consistent across groups such that each ISI pair used in a sham animal was used in a subsequent LFPI animal. One min after the final CS-US pairing (5 min total), mice were removed from context A and placed back in their home cage (see **Fig. 1** for schematic). Twenty four hours later (day 7)

animals underwent behavioral testing to measure threat responses in context B, a custom made triangular conditioning chamber with black striped Plexiglas walls and a smooth, opaque black plastic floor, scented with organic vanilla extract. Mice were allowed to freely explore the chamber for 1 min before experiencing 3 presentations of the CS alone (60s, interstimulus interval). Again, animals were removed from context B after a total of 5min. During testing, freezing behavior was scan sampled every 5th second from the onset of the first CS presentation to the end of the trial (4 min total). Freezing was defined as a total lack of movement aside from respiration at the instant of every 5th second. The total instance of freezing was then divided by total observations to generate a freezing percentage per animal. Behavioral data was collected from 26 animals (17 sham; 9 LFPI).

Electrophysiology

All electrophysiological experiments were performed on days 7-8 after injury or sham surgery. Slice preparation was performed as previously described (Johnson et al., 2014). Briefly, animals were anesthetized with isoflurane, the brain was dissected out and placed in ice-cold oxygenated (95%O_2 / 5%CO_2) sucrose-containing artificial cerebrospinal fluid (aCSF) containing (in mM): sucrose 202, KCl 3, NaH_2PO_4 2.5, $NaHCO_3$ 26, glucose 10, $MgCl_2$ 1, $CaCl_2$ 2. Coronal slices 300 μm thick were cut on a vibratome (VT1200S, Leica Microsystems, Buffalo Grove, IL, USA) and transferred to 33–37°C oxygenated (95%O_2 / 5%CO_2) control aCSF containing (in millimolar): NaCl 130, KCl 3, NaH_2PO_4 1.25, $NaHCO_3$ 26, glucose 10, $MgCl_2$ 1, $CaCl_2$ 2. Slices were allowed to incubate for at least 60 min before recording. VSD imaging and field potential

recordings were performed in an interface chamber, intracellular recordings were performed in a submersion chamber, both with a flow rate of approximately 2.0 ml/min and maintained at 27–30°C. Brain slices for recording were consistently selected from the same rostral-caudal region of the amygdala that exhibited a pear shaped basolateral amygdala (BLA) contiguous with an ovoid central amygdala (CeA), as seen in **Figs. 2&3**. This rigid criterion resulted in 1-2 brain slices per animal. Brain slices were hemisected prior to recording and only slices from the hemisphere ipsilateral to the site of injury were used. Our laboratory has previously demonstrated that contralateral slices are altered by LFPI and thus do not serve as an appropriate control for the injured hemisphere (Tran et al., 2006). For single cell recordings, a maximum of 1 cell per brain slice was used for analysis.

Field excitatory post synaptic potential recording (fEPSP) electrodes were fabricated from borosilicate glass (World Precision Instruments, Sarasota, FL, USA, #1B150F-4) pulled to a tip resistance of 2-6 MΩ and filled with aCSF. Field potentials were recorded in the central region of the BLA (**Fig. 2**) with an Axoclamp 900A amplifier and pClamp10 data acquisition software (Molecular Devices, Sunnyvale, CA, USA), filtered at 2 kHz. Stimulating electrodes were non-concentric bipolar (World Precision Instruments, Sarasota, FL, USA, #ME12206) and placed in the dorsal most portion of the lateral amygdala (LA), just medial of the external capsule. Electrical stimuli were 100 μs in duration. Field potential input-output relationships (50-500 μA stim, 50 μA increments, 8 s inter stimulus interval) and paired-pulse ratios (200uA stim, 75 ms inter stimulus interval, 8 s inter-pair interval) were performed prior to VSD

recordings. Field potential recordings were also recorded simultaneously with VSD recordings. The inter-stimulus interval for field potentials recorded during the VSD trials was 20 s. This duration was necessary to accommodate the every other trial subtraction method used for VSD analysis. Simultaneous VSD and field recordings were performed at 100 μA, 200 μA and 300 μA stimulation intensities in aCSF. Only the 200 μA stimulation intensity was used for experiments using various pharmacological manipulations. All figures and statistics reported in the manuscript are based on the 200 μA stimulation intensity data. However, see **Table 1** for data and statistics generated from all stimulation intensities. The 200 μA stimulation intensity was chosen because it elicits an approximately half maximal field potential response, while providing a high enough signal to noise ratio for VSD analysis. A subset of brain slices underwent field potential recordings and/or VSD imaging in the presence of 50 μM D-(-)-2-Amino-5-phosphonopentanoic acid (APV) + 6 μM 6-Cyano-7-nitroquinoxaline-2,3-dione (CNQX) to suppress ionotropic glutamatergic transmission, 0.4 μM TTX to block voltage-gated sodium channels, or 1 μM CGP 55845 to antagonize $GABA_B$ receptors. Field potential data was analyzed using pClamp10 and in house, custom written MATLAB scripts.

Whole-cell patch-clamp current-clamp recording electrodes were fabricated from borosilicate glass (World Precision Instruments, Sarasota, FL, USA, #1B150F-4) pulled to a tip resistance of 4–7 MΩ and filled with an internal solution containing (in milimolar): KGluconate 145, KCl 2.5, NaCl 2.5, HEPES 10, $MgCl_2$ 2, ATP.Mg 2, GTP.Tris 0.5, and BAPTA .1. Whole-cell recordings of BLA pyramidal neurons were performed using a Multiclamp 700B amplifier and pClamp10 data acquisition software

(Molecular Devices, Sunnyvale, CA, USA). All current-clamp recording voltages were corrected for a liquid junction potential calculated at −14.5 mV (using the Junction Potential utility in Clampex 10.3), and a series voltage error of 2.2 mV. The resting membrane potential was measured immediately following break in, and then current was injected to bring cells to the target holding/resting membrane potential of -78mV. Target membrane potential value was chosen empirically based on the resting membrane potential of initial whole cell recordings. Measures of intrinsic excitability were gathered from a series of hyperpolarizing and depolarizing current injections through the whole-cell recording electrode (-50-225 pA , 25 pA increments, 8s inter step interval). BLA pyramidal neurons were identified on the basis of previously characterized morphological and physiological properties (Sah et al., 2003). Whole-cell current-clamp data was analyzed using pClamp10 software.

Voltage-Sensitive Dye Imaging Acquisition

Voltage-sensitive dye imaging (VSD) acquisition using Neuroplex software was performed as previously described (Johnson et al., 2014). Briefly, VSD dye di-3-ANEPPDHQ (Invitrogen) was prepared at a working concentration of 67 μg/ml in aCSF and applied to slices for 16 min. The slices were subsequently rinsed in standard aCSF and transferred to the interface recording chamber. The dye was excited by seven high-power green LEDs (Luxeon Rebel LXML-PM01-0100, Philips) coupled to a 535 ± 25 nm bandpass filter and 565 nm dichroic mirror. Fractional changes in VSD fluorescence (ΔF/F) were isolated with a 610 nm longpass filter and recorded at 1.0 kHz with a fast video camera with 80 × 80 pixel resolution (NeuroCCD, Redshirt Imaging, Decatur, GA,

USA) through a reverse-lens macroscope with a 50 mm f/1.3 M46 lens (Dark Invader). Each camera pixel imaged a 25 μm × 25 μm region of tissue. The green light stimulus was triggered 230 ms prior to fluorescence acquisition, followed by electrical stimulation 170 ms after onset of fluorescence acquisition. All VSD recordings were 13 trials, 1.0 s in duration (1000 samples), with a 20 s interval between electrically stimulated trials. Each stimulated trial was followed 10 s later, by a non-electrically stimulated trial that was used to subtract photo-bleaching from the active signal (see below for details).

Voltage-Sensitive Dye Imaging Analysis

Each individual VSD trial used to create brain slice averages, was manually reviewed for ambient light contamination and gross abnormalities; if present, these trials were excluded from further analysis. Initial processing was performed as described in (Johnson et al., 2014). Fractional change in fluorescence values (ΔF/F) was calculated as follows: fluorescence values for each pixel in each trial were normalized according to the average fluorescence in the pixel during a 64 ms window immediately preceding the electrical stimulus. Then, the average from the corresponding pixel in the non-electrically stimulated trial was normalized and subtracted from the individual electrically stimulated trials to correct for photo-bleaching. VSD recordings were filtered in x and y spatial coordinates by convolution with a 5 pixels × 5 pixels Gaussian filter (Σ = 1.2 pixels), and in time by convolution with a five sample median filter. No additional filtering was applied to any of the images or analysis of VSD data. For VSD videos and representative movie frames, the ΔF/F for each pixel for the given sample (ms) is displayed as pseudocolor superimposed onto the image of the brain slice. Time points selected for the

representative movie frames in (**Fig. 3**), correlate to florescence peaks analyzed in the regional average line plots (**Fig. 3&4**). Peaks maps (**Fig. 5**) were generated by pseudocoloring and plotting the maximum ΔF/F value of any sample at each pixel.

Raster plot construction, analysis, and statistics were performed using the MATLAB VSD analysis toolbox provided by and described in (Bourgeois et al., 2014). To begin raster construction, regions of interest (anatomical regions) were defined for segmentation. In these experiments, the anatomical boundaries of central amygdala (CeA) and basolateral amygdala (BLA) were clearly visible and used to draw region boundaries. There was no clear, reliable anatomical boundary separating lateral and basal amygdala in our images, thus they were combined into the "BLA" region for analysis, unless specifically stated. However, the BLA was further divided into medial (BLA(m)) and lateral (BLA(l)) sections. Medial and lateral BLA were analyzed separately as they are physiologically distinct, in that they receive differential inputs from other brain regions and sit in a different position along the general dorsoventral, lateromedial directionality of amygdala inter-nuclear signaling (Sah et al., 2003; Duvarci and Pare, 2014). Regions were then split into 100 μm segments along the dorsoventral axis, numbering segments in ascending order from dorsal to ventral location (see **Fig. 3**). Average ΔF/F vales were calculated for each spatiotemporal site and plotted as pseudocolor in the distance from stimulating electrode versus time raster plots. To account for slight variability in region of interest size when creating average raster plots, all individual slice raster plots were stretched or compressed to have the same number of

segments. That number was set as the mean number of segments from the individual slices (CeA = 6, BLA(m) = 12, BLA(l) = 12).

Statistical comparison of group raster plots was performed at each individual spatiotemporal site using a permutation test (t=1000). Permutation is a nonparametric test that randomly resamples data to generate a null distribution describing variability in the data. Significant differences ($\alpha < .05$) are registered at sites where the experimental versus control groupings explain the variability in the data. The p-values generated are displayed in pseudocolor on a p-value heat-map (**Fig. 4A row 4**). To clarify areas of significant difference between average raster plots, the sham raster plot was subtracted from the LFPI raster plot, and only the $\Delta F/F$ differences at sites with $p = < 0.05$ are plotted (**Fig. 4A row 3**).

Multi-segment regional averages were calculated and used to create line plots (**Fig. 3&4**). Line plots show the average $\Delta F/F$ (dark line) surrounded by SEM ellipses (shaded surrounding). The segments selected for line plots were the same between conditions and consistent by region (CeA = seg 1-3, BLA(m) = seg 2-6, BLA(l) = seg 2-6). To look at signal propagation through the amygdala circuit we assessed the ratio of activation in the lateral amygdala (LA) compared to the basal amygdala (BA) or CeA. The quantification of activation for these ratios, seen in (**Fig. 5B&C**) is based on fast depolarizing peak (FDP) values from multi-segment averages within each region. The LA region was defined as a combination of segments 1-3 of both BLA(m) and BLA(l). The BA region was defined as a combination of segments 7-10 of both BLA(m) and BLA(l).

The CeA region was viewed in its entirety (segments 1-6) for this analysis, as we were interested in both the magnitude and distance of signal propagation. VSD analysis was performed using a combination of Neuroplex, custom MATLAB scripts, and GraphPad Prism. VSD/electrophysiological data was collected in 74 slices prepared from 41 animals.

Statistical Procedures

All statistical analyses and calculations were performed using MATLAB and/or GraphPad Prism. *A priori* power calculations were performed using G*Power (Faul et al., 2007) based on variability from similar previous experiments. All statistical tests for significance were conducted using Mann-Whitney U-tests, two-way repeated-measures ANOVA with Sidak's multiple comparison test in order to test for injury effect and stimulation intensity effect or the permutation test described in (Bourgeois et al., 2014), where applicable. Statistical significance was $P < 0.05$ ($P < 0.05$*, $P < 0.01$**, $P < 0.001$***). N values are reported per brain slice and per animal, where appropriate, with a maximum of 2 slices per animal. For physiological experiments (fEPSP and VSD) when multiple brain slices from a single animal were used, data from individual brain slices generated from the same animal were averaged yielding a single animal value for each given measure. The value generated was used in group analysis and statistics, based on the animal N. For pharmacological manipulation pre vs. post drug wash comparisons, slices were considered independent samples, used for analysis and statistics, based on the slice N. Data in the figures are presented as group means ± SEM.

Results:

LFPI causes a decreased threat response to cued fear conditioning

In order to assess the potential effects of LFPI on amygdala dependent behaviors, mice were tested using a combined auditory and visually cued fear conditioning response paradigm. It is well established that amygdala activity plays an essential role in the acquisition and expression of light and/or tone cued threat response (Phillips and Ledoux, 1992; Ledoux, 2000; Newton et al., 2004; Duvarci and Pare, 2014). While it is traditional to refer to the behavioral response in this paradigm as fear, the authors note that freezing behavior is better defined as a threat response based on survival instinct, rather than a subjective or conscious feeling of fear (LeDoux, 2012). Mice were randomly assigned to, and underwent, either sham or LFPI procedures prior to fear conditioning and retrieval testing. On day 6 after injury animals underwent a conditioning period in context A where they were exposed to 3 presentations of the CS-US (light/tone-foot shock) pairing. On day 7 animals were placed in a novel context (context B) and exposed to 3 presentations of the CS (light/tone) alone. Freezing behavior was assessed from the onset of the first CS presentation to the end of the trial and expressed as percent of time freezing (**Fig. 1A**) (see methods for full details). During the testing period LFPI animals froze significantly less than sham animals, indicating a deficit in acquisition and/or expression of threat response (**Fig. 1B,** sham = 50%, 95% CI 46.47-57.94% n=17, LFPI = 33.33%, 95% CI 27.9-37.38% n=9; P <0.001).

Decreased network excitability in the amygdala following LFPI

After identifying LFPI-induced deficits in amygdala-dependent behaviors we investigated amygdala function for putative physiological substrates contributing to the observed behavioral deficits. To begin assessing the effects of LFPI on amygdala physiology we recorded *ex vivo* extracellular field excitatory post synaptic potentials (fEPSP) from the central region of the basolateral amygdala (BLA) in coronal brain slices. Field EPSP recordings contain both a fiber volley (FV), representing the presynaptic action potentials and an extracellular field potential response, which is predominantly the postsynaptic dendritic component of the signal. BLA field potentials were evoked via electrical stimulation of the lateral amygdala (LA) and external capsule, the primary input of sensory information into the amygdala (Ledoux, 2000; Sah et al., 2003) (**Fig. 2, Experimental set-up**). Field EPSP responses were recorded over a range of stimulation intensities to construct input-output curves (I/O), and simultaneous to VSD recordings. Representative field potential recordings in **Fig. 2A** show the drastic decrease observed in fEPSPs in slices from LFPI animals. Brain slices from LFPI animals demonstrate a significant downward shift in the I/O curve (**Fig. 2B,** sham n=16 slices / 10 animals, LFPI n=14 slices / 7 animals, two-way repeated-measures ANOVA, (injury effect) F (1,15) = 18.66; P <0.001). Additionally, brain slices from LFPI animals showed a significant decrease in fEPSPs recorded simultaneously with VSD recordings (**Fig. 2C,** sham 0.458 95% CI 0.368-0.678 mV/ms n=17 slices / 10 animals, LFPI 0.148 95% CI 0.049-0.305 mV/ms n=14 slices / 7 animals; P =0.002). Interestingly, LFPI does not appear to alter transmitter release probabilities as there was no significant difference in the paired pulse ratio when a second stimuli was delivered shortly after the first (**Fig. 2D,** sham 0.470 95% CI 0.289-0.645 n=14 slices / 8 animals, LFPI 0.424 95% CI 0.302-0.661

n=12 slices / 7 animals, *P*= 0.999). Bath application of APV (50 μM) and CNQX (6 μM) decreased fEPSPs to a level indistinguishable from noise (fEPSP slope post APV/CNQX = 0.005 95% CI -0.002-0.008 mV/ms n=10 slices) and isolated the presynaptic FV responses. There was no significant difference in FV amplitude recorded in the presence of APV/CNQX between slices from sham and LFPI animals (**Fig. S1**, sham 0.267 95% CI 0.167-0.376 mV n=8 slices / 6 animals, LFPI 0.279 95% CI 0.107-0.381 mV n=6 slices / 4 animals; *P*= 0.695). This suggests that LFPI has little or no effect on the number of neurons or axons directly activated by the stimulating electrode. Both FV and fEPSP responses were blocked by bath application of TTX (0.4 μM) (**Fig. S1**).

In order to more fully understand and visualize the effects of LFPI on amygdala physiology and circuit function, we performed a series of voltage sensitive dye (VSD) imaging experiments. VSD imaging allows for the recording of changes in voltage in hundreds or thousands of neurons in all sub-regions of the amygdala simultaneously. This not only allows for the evaluation of the spatiotemporal dynamics of amygdala circuit activation, but to also directly view inhibition as areas of regional hyperpolarization. VSD shows relative changes in voltage by recording fractional changes in fluorescence (ΔF/F) emitted by voltage sensitive dyes. When used in the hippocampal brain region, this voltage sensitive dye (di-3-ANEPPDHQ) fluorescence has a linear correlation to neuronal membrane voltage (V_m), where 1 x 10^{-4} ΔF/F equals a roughly 1 mV change in V_m (Ang et al., 2006). For this reason all ΔF/F values are reported in (10^{-4}) notation. **Figure 3A** again shows the experimental setup and representative VSD movie frames from slices from sham and LFPI animals (see also **Video S1** and **Video S2** in

supplemental materials). A post injury decrease in the intensity and duration of depolarization throughout the amygdala can be seen in the representative movie frames as fewer red and orange pixels at 6 ms and 56 ms. An increased delayed hyperpolarization is also apparent as an increase in blue pixels in BLA at the 306 ms time point. In order to interpret group data, VSD videos were used to create regional raster plots and multi segment regional average line plots for analysis (see methods for full details). **Figure 3B** shows an example of how anatomical amygdala regions were defined and segmented for rasterization. The amygdala was separated into three regions for analysis, central amygdala (CeA), medial basolateral amygdala (BLA(m)) and lateral basolateral amygdala (BLA(l)). The same rostral-caudal region of amygdala (1-2, 300 μm brain slices) that exhibited a pear shaped BLA contiguous with an ovoid CeA was used in every animal. **Figure 3C** shows a typical VSD regional average line plot response profile, in a slice from a sham animal, containing the three distinct peaks ultimately used in analysis. There is an initial fast depolarizing peak (FDP = max ΔF/F 0-35 ms), followed by a secondary slow depolarizing peak (SDP = max ΔF/F 36-136 ms) and a delayed hyperpolarization or slow negative-going peak (SNP = minimum ΔF/F 137-600 ms). In all regional line plots the dark line is the average ΔF/F surrounded by a shaded standard error of the mean (SEM) ellipse.

The group data presented in **Figure 4** (VSD response to 200 μA stimulation of LA) reveals the profound alterations in amygdala physiology following LFPI. Rows one and two of **Figure 4A** show the average group raster plots for slices from sham and LFPI animals in all three amygdala subregions. In these raster plots warm colors (yellow to

red) represent depolarization and cool colors (blue to purple) represent hyperpolarization. Row three is a difference raster showing the magnitude and direction of difference between sham and LFPI raster plots at each spatiotemporal site. Row four shows the results of a permutation test used to compare sham and LFPI raster plot data, displaying a *P* value at each spatiotemporal site to denote where differences between slices from sham and LFPI animals are significant (see methods for full details). All three amygdala regions show an LFPI-induced decrease in the intensity and duration of the depolarizing response to electrical stimulation and an increase in delayed hyperpolarization 200-400 ms after stimulation. This is particularly evident in the BLA(m) raster plots. We then measured and compared the aforementioned peak ΔF/F values from each amygdala region in response to 200 μA stimulation. In CeA, LFPI caused a significant decrease of the FDP and SNP (**Fig. 4B, Table 1**). Interestingly there is no clear SDP in CeA, thus it was not analyzed. In BLA(m) LFPI caused a significant decrease of the FDP, SDP and SNP (**Fig. 4C, Table 1**). In BLA(l) LFPI caused a significant decrease in the FDP and SNP, but had no effect on the SDP (**Fig. 4D,Table 1)**. These experiments were repeated at 100 μA and 300 μA stimulation intensities, both of which maintained a similar trend of decreased activation in LFPI animals. All peak values and statistical comparisons are reported in **Table 1**.

In order to isolate and remove the ionotropic glutamatergic component of the VSD signal a separate set of VSD experiments were performed in the presence of glutamatergic antagonists (APV 50 μM, CNQX 6 μM). When glutamatergic transmission was suppressed the magnitude of the ΔF/F difference between sham and LFPI animals, at

both depolarizing peaks, was drastically decreased throughout and eliminated in certain regions (**Table S1, Fig S2)**. While the blockade of excitatory neurotransmission substantially reduces the magnitude of the depolarization difference between brain slices from sham and LFPI animals, a significant depression of the fast depolarization in BLA(m) in brain slices from LFPI animals remains (**Fig. S2B&C,** sham 3.54 95% CI 2.84-4.12 x 10^{-4} ΔF/F n=10 slices / 7 animals, LFPI 2.41 95% CI 1.96-2.87 x 10^{-4} ΔF/F n=12 slices / 6 animals; *P*= 0.008). This suggests an additional component of the remaining VSD signal, possibly GABAergic inhibition, is also altered by LFPI.

Amygdala circuit dysfunction following LFPI

Diminished amygdala network excitability as expressed by a decrease in fEPSP and VSD depolarization could be due to a decrease in activation of the primary input into the amygdala (LA/external capsule), a decrease in propagation of that signal through the amygdala circuit, or a combination of both. While the LFPI-induced decrease in depolarization adjacent to the stimulating electrode (visible in representative movie frames & and group raster plots) demonstrates a decrease in activation of the primary input, it is still unclear if propagation through the amygdala circuit is affected by LFPI. Therefore, to better understand the spatial component or spread of the stimulus evoked response, peak maps were created to show the max ΔF/F at any time point in each pixel to isolate the pattern of maximal depolarization through the amygdala. Further, by using multiple stimulation intensities we can determine how increasing activation of the input affects the spatial component of activation in brain slices from sham and LFPI animals. Reduced depolarization and spread of activation from lateral amygdala to basal or central

amygdala can be seen in the representative peak maps of slices from LFPI animals (**Figure 5A)**.

Based on the apparent decrease in spread of depolarization after LFPI, we next sought to examine the propagation of activity through the amygdala circuit. In order to normalize differences in activation of the primary input (lateral amygdala) and isolate propagation of activity, we used the FDP from the different amygdala regions to create ratios of activation, a method originally described in (Avrabos et al., 2013). The amygdala circuit propagates signals in a dorsoventral, lateromedial fashion, beginning in the lateral amygdala (LA) and moving towards the medial portion of CeA. Thus, an important measure of amygdala circuit function or strength is what percentage of depolarization in LA is propagated to basal amygdala (BA) and/or CeA. For this analysis, LA was defined as a combination of raster segments 1-3 of both BLA(m) and BLA(l), the BA region was defined as a combination of raster segments 7-10 of both BLA(m) and BLA(l), and the CeA region was viewed in its entirety (segments 1-6). BA and CeA FDP response amplitudes to various stimulation intensities were divided by the corresponding LA FDP amplitude to create activation ratios that express the relative strength of LA-to-CeA or LA-to-BA signaling in slices from sham and LFPI animals. Amygdalae of LFPI animals exhibit a significant decrease in the ratio of activation between LA-to-BA (**Fig. 5B,** sham n=16 slices / 9 animals, LFPI n=14 slices / 7 animals, two-way repeated-measures ANOVA, (injury effect) F (1,14) = 10.89; P = 0.005) and LA-to-CeA (**Fig. 5C,** sham n=16 slices / 9 animals, LFPI n=14 slices / 9 animals, two-way repeated-measures ANOVA, (injury effect) F (1,14) = 12.77; P= 0.003). Taken together with previous

measures of network excitability, this data suggests there is both a decrease in the excitability of the primary input to the amygdala together with a decrease in signal propagation through the amygdala circuit following LFPI.

Late hyperpolarization in VSD signal mediated via $GABA_B$

To further investigate the putative contribution of $GABA_{A\ and\ B}$ to the late hyperpolarization component of the VSD signal, VSD recordings were performed in brain slices from naïve animals treated with the $GABA_B$ antagonist GCP55845 (1 μM). As seen in **Table S1** and **Supplementary figure S3,** application of CGP55845 completely abolishes the late hyperpolarization, revealing a persistent depolarization similar to the transmembrane voltage response of stimulated glia (Leung and Zhao, 1995). Analysis of the average ΔF/F signal shows that CGP55845 has a small but significant effect on the FDP (**Fig. S3B&C,** pre-CGP 13.3 95% CI 11.6-14.8 x 10^{-4} ΔF/F, post-CGP 17.1 95% CI 14.1-19.3 x 10^{-4} ΔF/F n=5 slices; *P*= 0.03), perhaps due to the presynaptic activity of $GABA_B$ (Yamada et al., 1999), and a drastic effect on the SNP (**Fig. S3B&C,** pre-CGP .571 95% CI -.471-.86 x 10^{-4} ΔF/F, post-CGP 6.0 95% CI 4.88-7.47 x 10^{-4} ΔF/F n=5; *P*= 0.008).

BLA pyramidal neuron intrinsic excitability is unaltered by LFPI

To determine if the LFPI induced differences seen in VSD imaging and fEPSP recordings were due to a change in the intrinsic properties of amygdala principal neurons, we performed a series of whole-cell current-clamp recordings of BLA pyramidal neurons

in brain slices from sham and LFPI animals. To begin, we assessed the passive membrane properties of amygdala neurons that effect the fractional changes in fluorescence measured in VSD recordings. Resting membrane voltage (Vm) measured immediately following break in was unaffected by LFPI (**Fig. 6C,** sham -78.05 95% CI -80.97--75.28 mV n=8, LFPI -79.45 95% CI -81.8--77.1 mV n=8; *P*= 0.49). Furthermore, there was no significant difference in the input resistance (R_{in}) of BLA pyramidal neurons in slices from sham and LFPI animals (**Fig. 6D,** sham 118.6 95% CI 99.56-151.7 MΩ n=8, LFPI 133 95% CI 112.2-144.9 MΩ n=8; *P*= 0.78). Next, a series of depolarizing current injections were used to assess intrinsic excitability. Action potential threshold (**Fig. 6E,** sham -53.79 95% CI -56.4--52.18 mV n=8, LFPI -52.78 95% CI -54.5--51.18 mV n=8; *P*= 0.32) and frequency in response to depolarizing current were not significantly different in BLA neurons from sham and LFPI slices (**Fig. 6B,** sham n=8 LFPI n=8, two-way repeated-measures ANOVA, (injury effect) $F(1,14) = .09628$; $P = 0.76$).

Discussion:

Neuropsychiatric symptoms are highly prevalent in mTBI patients and represent some of the most prolonged and debilitating symptoms associated with mTBI (McAllister, 1992; Tateno et al., 2003; Jorge et al., 2004; Malkesman et al., 2013). In this study we have taken the first steps towards understanding how mTBI disrupts circuit level function in the amygdala, a brain region crucial for processing emotional stimuli. Initially, we explored amygdala-dependent behaviors 7 days post-LFPI, demonstrating a significant deficit in threat response in a cued fear conditioning paradigm. We next characterized LFPI-induced alterations in amygdala physiology using a combination of electrophysiological and voltage sensitive dye imaging (VSD) techniques. We discovered significant decreases in network excitability and activation throughout several amygdala sub-regions. Furthermore, leveraging the spatial information provided by VSD imaging we establish that in addition to the primary input to the amygdala being less excitable, there is also a congruent decrease in signal propagation of activation through the amygdala circuit. Finally, we preformed a series of whole-cell current-clamp recordings demonstrating that the intrinsic excitability and membrane properties of BLA pyramidal neurons are unaltered by LFPI. Together these data suggest that LFPI causes robust circuit level dysfunction in the amygdala associated with an altered behavioral response to threatening stimuli.

Many previous reports have shown opposing effects in amygdala associated behaviors following mTBI (Reger et al., 2012; Malkesman et al., 2013). A recent publication by Reger et al. reported enhanced fear conditioning 4 days post LFPI in rats.

Potential reasons for the heterogeneity in results using animal models is likely due to subtle differences in technique, experimental time point, injury models, and animal strains used. Similarly, the array of neuropsychiatric symptoms present in mTBI patients is likely the consequence of the heterogeneity of physical insults suffered by the brain that result in mTBI and a variety of other environmental factors. It is certainly feasible that different animal brain injury protocols are simply modeling different mTBI patient populations or post-injury time points, rather than producing contradictory results. For our study we chose a well-established behavioral task (cued fear conditioning), in which the threat response (freezing behavior) is directly associated with activation of the medial portion of central amygdala (Phillips and Ledoux, 1992; Ledoux, 2000; Duvarci and Pare, 2014). Our injury model produced a consistent and robust decrease in freezing behavior in a cued fear conditioning paradigm at 7 days post-LFPI. While increases in anxiety and fear response are often associated with mTBI it is important to note that depression/apathy is at least as prevalent as anxiety disorders in human mTBI patients (Jorge et al., 2004; Malkesman et al., 2013). Furthermore, it is conceivable that the observed behavioral deficit is only present acutely (7 days after injury) and could progress to heightened fear response or anxiety at protracted time points.

As a decrease in freezing behavior in a cued fear response paradigm is typically associated with decreased network excitability in the amygdala, we hypothesized that amygdala excitability would be diminished as a result of LFPI. In order to test this hypothesis we performed a series of electrophysiological and VSD experiments. Basolateral amygdala (BLA) fEPSP responses evoked by lateral amygdala (LA)

stimulation, revealed a significant decrease in network excitability, as measured by fEPSP input/output curves following LFPI. Interestingly, paired-pulse stimulation was not significantly altered by LFPI, suggesting that a change in probability of vesicular release did not occur. Furthermore, the pre-synaptic fiber volley was also unchanged by LFPI, implying that the number of neurons activated by the stimulating electrode was not different in slices derived from sham and LFPI animals. The lack of in injury effect on the intrinsic properties of BLA pyramidal neurons further supports the conclusion that a similar number of principal cells were activated in brain slices from sham and LFPI animals. Overall these results suggest that LFPI disrupts the balance between excitation and inhibition in the amygdala via mechanisms other than a change in probability of release or large scale excitatory cell loss, likely through a perturbation of the critical balance between glutamatergic and GABAergic transmission seen in other brain regions following LFPI (Witgen et al., 2005; Cole et al., 2010).

To further probe amygdala circuit function and examine the spatiotemporal dynamics of activation throughout all amygdala sub-regions, we performed a series of VSD experiments. These experiments corroborated fEPSP data revealing a strong LFPI-induced decrease in the fast depolarizing component in all amygdala sub-regions. Once we determined that LFPI causes a significant decrease in amygdala network excitability, we were further interested in determining if this decrease was due to a decreased ability to excite the primary input of the amygdala (LA), a decrease in the propagation of the signal through the amygdala circuit, or both. The LFPI-induced decrease in depolarization adjacent to the stimulating electrode (visible in representative movie

frames & and group raster plots) shows a decrease in activation of the primary input. By normalizing the amount of activation adjacent to the stimulation electrode we were able to determine the percentage of activation of the primary input of the amygdala (LA) that was propagated to distal regions of BA or the primary output of the amygdala i.e., the CeA. This revealed that not only is the LA less excitable after injury, but the relative circuit strength of LA-to-CeA and LA-to-BA projections are also weakened by LFPI.

The fast depolarizing response of the VSD signal is thought to be a mixed signal including action potential firing, glutamatergic and GABAergic transmission (Tominaga et al., 2000; Carlson and Coulter, 2008). Notably, this decrease in FDP was present in the central amygdala, which projects directly to autonomic brain stem structures responsible for the freezing behavior measured in the cued fear conditioning paradigm (Sah et al., 2003; Duvarci and Pare, 2014). The typical observed VSD response had two or three distinct peaks, depending on region, the aforementioned fast depolarizing peak (FDP), a protracted slow depolarizing peak (SDP), and a late slow negative peak (SNP) (**Fig. 3C**). The FDP is most commonly assessed as a measure of activation/excitation and is the best characterized portion of the VSD signal. The SDP and SNP are likely heavily influenced by gliotic activation, which is proportional to the initial depolarization (Leung and Zhao, 1995). Thus, differences in these peaks could simply be a consequence of the differences observed in the preceding FDP. However, $GABA_B$ is playing a large role in the generation of the SNP (see **Fig. S3**) and could be contributing to the differences in late hyperpolarization between slices from sham and LFPI animals. Further, the observation that an LFPI-induced decrease in the FDP and SDP persists in the presence of

glutamatergic antagonists suggests that other intrinsic and/or extrinsic components of the amygdala circuit are affected by LFPI. While the current study does not directly assess GABAergic inhibition in the amygdala, previous findings from our laboratory demonstrated an increase in inhibition from CCK positive interneurons in area CA1 of the hippocampus, 7 days post LFPI (Johnson et al., 2014). It is possible that CCK positive inhibitory interneurons present in the BLA have a similar response to LFPI and contribute to the decrease in amygdala network excitability demonstrated in this study.

We next examined the intrinsic properties of BLA pyramidal neurons to determine if the LFPI-induced decrease in excitability seen in fEPSP and VSD recordings was a consequence of changes in the intrinsic excitability of the principal excitatory cell type within the BLA. Whole-cell current-clamp recordings of BLA pyramidal neurons revealed no changes in passive membrane properties or measures of intrinsic excitability following LFPI. As the amygdala nuclei are somewhat distal from the site of injury this finding, while not completely unexpected, does further elucidate a possible mechanism of the decrease in amygdala activation following LFPI. Taken together with FV and VSD in the presence of glutamatergic antagonists results, these experiments suggest that LFPI decreases excitability in the amygdala via a perturbation of glutamatergic transmission and likely other neurotransmitter/neuromodulator systems.

In summary, our data demonstrates that LFPI causes substantial perturbation of the balance between excitation and inhibition within the amygdala circuit, resulting in a decrease in network excitability of the basolateral amygdala and weakening of

dorsoventral-lateromedial internuclear amygdala projections. Further, this decrease in amygdala network excitability correlates to a depression in threat response behavior. To our knowledge this is the first study demonstrating the comprehensive effects of LFPI on amygdala circuit function and strength. This work highlights promising new sites of study towards understanding the mechanism LFPI-induced amygdala dysfunction and for the development of therapeutics targeted at mitigating or ameliorating mTBI-induced amygdala circuit dysfunction.

Acknowledgments:

This work was supported in part by NIH grants R37 HD059288 and RO1 NS069629. The authors would like to thank Drs. Gordon Barr and Colin Smith for critiquing and earlier version of this manuscript.

Table Legends:

Table 1: Group median peak ΔF/F values, 95% confidence intervals and *P* values for all peaks at all stimulation intensities. All ΔF/F values reported are the given value times 10^{-4}. Mann-Whitney U-test *P* values are reported for individual peak comparisons between sham and LFPI. For measures that were repeated at multiple stimulation intensities the two-way repeated-measures ANOVA, (injury effect comparison) are reported in the two right most columns. For all comparisons Sham n=16 brain slices from 9 animals, LFPI=14 brain slices from 7 animals. If there were multiple brain slices from the same animal the results were averaged and counted as a single n for analysis and statistics.

Table S1: Group median peak ΔF/F values and *P* values for all amygdala regions in the presence of APV+CNQX or pre and post CGP 55845. All ΔF/F values reported are the given value times 10^{-4}. Mann-Whitney U-test *P* values are reported for individual peak comparisons between sham and LFPI or pre and post CGP 55845.

Figure Legends:

Fig. 1 LFPI decreases freezing in a cued fear conditioning paradigm. (A) Animals are trained in context A on day 6 after injury and tested in a novel context (context B) on day 7 (CS- 75dB white noise and yellow light pulses flickering at 4 Hz, 20 s; US- 1.05 mA footshock, 1.5 s). The inter stimulus interval (ISI) was between 15-105 s with a trial mean of 60s, meaning the first and second ISI always added up to 120 s. (**B)** Percent of time freezing after presentation of CS on day 7. LFPI animals freeze significantly less after injury (sham n=17, LFPI n=9, P <0.001***).

Fig. 2 LFPI decreases lateral amygdala evoked basolateral amygdala fEPSPs. (A) Representative fEPSP recordings from brain slices of sham (green) and LFPI (red) animals (200 μA stimulation intensity). **(B)** Average fEPSP slope input-output (I/O) curve (50-500 μA, 50 μA steps, stimulation). LFPI causes a significant decrease in the BLA I/O curve (sham n=16 slices / 10 animals, LFPI n=14 slices / 7animals, P <0.001***). Black line denotes repeated measures that are significantly different in post hoc comparisons. **(C)** Distribution of fEPSP slopes recorded simultaneously with VSD imaging experiments (200 μA stimulation). LFPI causes a significant decrease in the BLA fEPSP slope (sham n=17 slices / 10 animals , LFPI n=14 slices / 7animals, P <0.002**). **(D)** BLA fEPSP amplitude paired pulse ratio (200 μA stimulation, 70 ms inter stimulus interval). LFPI has no effect on BLA fEPSP paired puse ratio (sham n=14 slices / 8animals, LFPI n=12 slices / 7 animals, P= 0.999). **(Experimental set-up)** Representative brain slice showing amygdala subregions and electrode placements. "Stim" and "Record" arrows show placement of tip of stimulation and recording electrodes.

Fig. 3 Amygdala VSD imaging recording set-up and representative movie frames. (A) Representative VSD movie frames from slices of sham and LFPI animals. Video frames show experimental set up and voltage response of the amygdala to LA stimulation. ΔF/F values at each spatiotemporal point are displayed as pseudocolor and stacked to create a video representation (see corresponding videos in **Video S1** and **Video S2**) The pseudocolor scale bar below shows the correlation of colors displayed to ΔF/F values. The time points selected (6, 56, 306 ms) roughly correlate to the peak indices shown in **C**. **(B)** Representative slice showing example regions of interest and raster segmentation. **(C)** Representative group average, multi segment regional average line plot showing approximate location of the peaks used in analysis. The solid color line shows the mean values and the shaded area is a SEM ellipse.

Fig. 4 VSD average raster plots and multi segment regional averages showing LFPI-induced alterations in amygdala activation. (A) Rows 1 and 2: group average raster representation of sham (n=16) and LFPI (n=14) VSD responses. **Row 3**: difference raster showing magnitude of differences between sham and LFPI rasters. Sham raster was subtracted from the LFPI raster, and only the ΔF/F differences at sites with p = <0.05 are plotted. **Row 4**: *P* value heat map showing the results of a permutation test used to compare sham and LFPI rasters, displaying a *P* value for each spatiotemporal site. **(B-D)** Group average multi segment regional average line plots and graphs of peak ΔF/F values from sham (n=16 slices / 9 animals) and LFPI (n=14 slices / 7 animals) animals. (**B**) Central amygdala (CeA) (segments 1-3) from LFPI animals exhibit a decrease in depolarization (FDP, *P*=0.001**) and an increase in late hyperpolarization (SNP, *P* <0.001***). (**C**) Medial basolateral amygdalae (BLA(m)) (segments 2-6) from LFPI animals exhibit a decrease in depolarization (FDP, *P*=0.002**; SDP, *P*= 0.011*) and an increase in late hyperpolarization (SNP, *P*= 0.023*). (**D**) Lateral basolateral amygdalae (BLA(l)) (segments 2-6) from LFPI animals exhibit a decrease in depolarization (FDP, *P*= 0.042**) and an increase in late hyperpolarization (SNP, *P*= 0.042*).

Fig. 5 Amygdala VSD peak maps and regional activation ratios showing decreased propagation in amygdala circuit following LFPI. (A) Representative peak maps showing the maximum ΔF/F recorded at each spatial site at any time point, for brain slices from sham and LFPI animals. From left to right: slice image showing amygdala anatomy followed by peak response to 100, 200, and 300 μA stimulation intensities. **(B)** LA-to-BA activation ratio. BA FDP amplitude/LA FDP amplitude reveals a significant decrease in propagation of activation in LFPI animals (sham n= 16 slices / 9 animals, LFPI n=14 slices / 7 animals, *P*= 0.005**). **(C)** LA-to-CeA activation ratio. CeA FDP amplitude/LA FDP amplitude reveals a significant decrease in propagation of activation from lateral to central amygdala in LFPI animals (sham n= 16 slices / 9 animals, LFPI n=14 slices / 7 animals, *P*= 0.003**).

Fig. 6 BLA Pyramidal neuron intrinsic excitability. (A) Representative voltage response to current injection in cells from sham and LFPI animals (-50 & 200 pA current steps). **(B)** AP frequency in response to depolarizing current (-50-225pA) (*P*= 0.76). **(C)** Resting membrane potential measured immediately following break in (*P*= 0.49). **(D)** Input resistance calculated from hyperpolarizing current injections (*P*= 0.78). **(E)** Action potential threshold: Vm at which 1st evoked AP initiated independent of current step (*P*= 0.32). All comparisons were made between Sham (n=8 cells / 4 animals) and LFPI (n=8 cells / 5 animals).

Fig. S1 APV and CNQX isolated fEPSP fiber volleys. (A) Representative fEPSP recordings in standard aCSF (blue) and aCSF containing 50 μM APV + 6 μM CNQX (grey) (200 μA stimulation intensity). **(B)** Representative fEPSP recordings in aCSF containing 50 μM APV + 6 μM CNQX (grey) and aCSF containing 0.4 μM TTX (black) (200 μA stimulation intensity). In both insets, in the grey traces the pharmacologically isolated fiber volley is visible. **(C)** pharmacologically isolated average fiber volley amplitudes. There is no significant difference in fiber volley amplitude from sham and LFPI animals (sham n=8 slices / 6 animals, LFPI n=6 slices / 4 animals, P= 0.695).

Fig. S2 APV and CNQX All experiments performed in the presence of APV 50 μM and CNQX 6 μM **(A)** Row 1 and 2: group average raster representation of sham (n=10) and LFPI (n=12) VSD responses. Row 3: difference raster showing magnitude of differences between sham and LFPI raster plots. Sham raster plot was subtracted from the LFPI raster plot, and only the ΔF/F differences at sites with $p \leq 0.05$ are plotted. Row 4: *P* value heat map showing the results of a permutation test used to compare sham and LFPI rasters plots, displaying a *P* value for each spatiotemporal site. **(B&C)** Group average multi segment regional average line plots and graphs of peak ΔF/F values from brain slices from sham (n=10 slices / 7 animals) and LFPI (n=12 slices / 6 animals) animals. In the presence of glutamatergic antagonists, medial basolateral amygdalae (BLA(m)) (segments 2-6) from LFPI animals maintain a decrease in depolarization at the FDP (FDP, $P < 0.0082$*) and an increase in late hyperpolarization (SDP, $P < 0.035$*).

Fig. S3 CGP 55845 (A) Row 1 and 2: group average raster plot representation of Pre and Post_CGP55845 (n=5) VSD responses in brain slices from naïve animals. Row 3: difference raster plot showing magnitude of differences between sham and LFPI raster plots. Sham raster plot was subtracted from the LFPI raster plot, and only the ΔF/F differences at sites with $p \leq 0.05$ are plotted. Row 4: *P* value heat map showing the results of a permutation test used to compare sham and LFPI raster plots, displaying a *P* value for each spatiotemporal site. **(B&C)** Group average multi segment regional average line plots and graphs of peak ΔF/F values from Pre and Post_CGP55845 (n=5) brain slices. Medial basolateral amygdalae (BLA(m)) (segments 2-6) exhibit an increase in fast depolarization (FDP, $P < 0.05$*) and a decrease in late hyperpolarization (SNP, $P < 0.001$***).

Supplementary Videos (S1, S2): Representative voltage sensitive dye imaging videos of slices prepared from sham (Video S1 in Supplementary Material) and LFPI (Video S2 in Supplementary Material) animals. Each video frame represents 1 ms, and the playback speed is 15 frames per second. The pseudocolor scale is the same as that shown for the movie frames in **Figure 3.** Videos are 375 ms excerpts from the original 200 μA stimulation intensity recordings.

Tables:

Table 1

Region_Peak:	100uA Stimulation			200uA Stimulation			300uA Stimulation			ANOVA Stats (by region)	
ACSF	Sham (ΔF/F):	LFPI (ΔF/F):	p-value:	Sham (ΔF/F):	LFPI (ΔF/F):	p-value:	Sham (ΔF/F):	LFPI (ΔF/F):	p-value:	F values	P-value
BLA(m)_FDP	12.91	9.48	0.0012	17.77	12.42	0.0021	20.86	14.35	0.0033	F(1,14)= 19.94	0.0005
95% CI	11.94-14.14	7.74-10.96		15.59-19.71	10.82-14.79		18.07-11.84	11.84-17.32			
BLA(m)_SDP	6.87	5.89	0.0311	10.9	7.75	0.0115	10.53	7.69	0.0052	F(1,14)= 10.83	0.0054
95% CI	5.77-7.94	4.32-6.57		8.72-11.62	6.96-9.22		9.65-13.2	7.07-9.4			
BLA(m)_SNP	-0.64	-1.5	0.0962	0.87	-0.59	0.0229	2.41	0.21	0.0079	F(1,14)=7.5	0.016
95% CI	-1.22-.15	-2.02-.65		.09-2.65	-1.5-0.55		1.48-4.27	-0.84-1.59			
BLA(l)_FDP	8.83	8.49	0.4524	12.44	9.81	0.0416	15.68	10.68	0.0164	F(1,14)= 7.01	0.0191
95% CI	8.02-10.1	5.34-9.6		11.24-14.87	8.12-12.4		13.89-17.71	8.79-14.38			
BLA(l)_SDP	6.97	6.1	0.5848	10.09	8.63	0.2463	11.23	8.97	0.0545	F(1,14)= 3.26	0.0524
95% CI	6.15-8.12	4.75-8.28		8.77-11.62	7.55-10.47		9.48-13.84	7.61-10.32			
BLA(l)_SNP	-0.34	-0.51	0.5543	0.33	-0.16	0.0416	1.72	0.47	0.0229	F(1,14)= 5.422	0.0354
95% CI	-.74-.14	-1.05-.1		.09-2.32	-0.76-0.43		1.07-3.97	-.28-1.3			
CeA_FDP	8.27	5.4	0.0002	11.53	7.15	0.0012	12.95	7.56	0.0003	F(1,14)= 33.08	<0.0001
95% CI	7.41-9.44	4.38-6.1		10.09-12.85	5.63-8.64		11.69-14.37	6.16-9.42			
CeA_SNP	0.61	-0.13	0.0545	1.75	-0.21	0.0007	2.34	-0.12	0.0002	F(1,14)= 30.46	<0.0001
95% CI	-.11-.98	-.7-.5		1.05-2.25	-0.75-0.34		1.94-2.98	-.37-.76			

Table S1

Region_ Peak:	200uA Stimulation		
APV+CNQX	Sham(ΔF/F)	LFPI (ΔF/F):	p-value:
BLA(m)_FDP	3.54	2.41	0.0082
BLA(m)_SDP	3.41	2.55	0.035
BLA(m)_SNP	-0.6	-1.35	0.067
BLA(l)_FDP	3.08	2.39	0.014
BLA(l)_SDP	3.88	2.9	0.0221
BLA(l)_SNP	-0.13	-1.1	0.0315
CeA_FDP	2.07	1.6	0.046
CeA_SNP	-0.06	-0.51	0.5152
CGP-55845	PreCGP(ΔF/F):	PostCGP(ΔF/F):	p-value:
BLA(m)_FDP	13.32	17.12	0.0317
BLA(m)_SDP	10.85	11.58	0.4127
BLA(m)_SNP	0.57	6	0.0079
BLA(l)_FDP	9.01	11.71	0.2222
BLA(l)_SDP	9.91	11.11	0.4127
BLA(l)_SNP	0.21	4.7	0.0079
CeA_FDP	8.24	11.26	0.0556
CeA_SNP	0.95	3.49	0.0079

Figures:

Figure 1

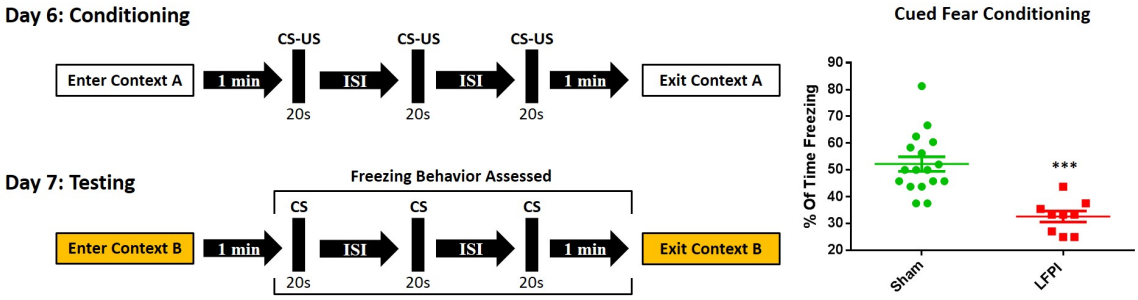

Figure 2

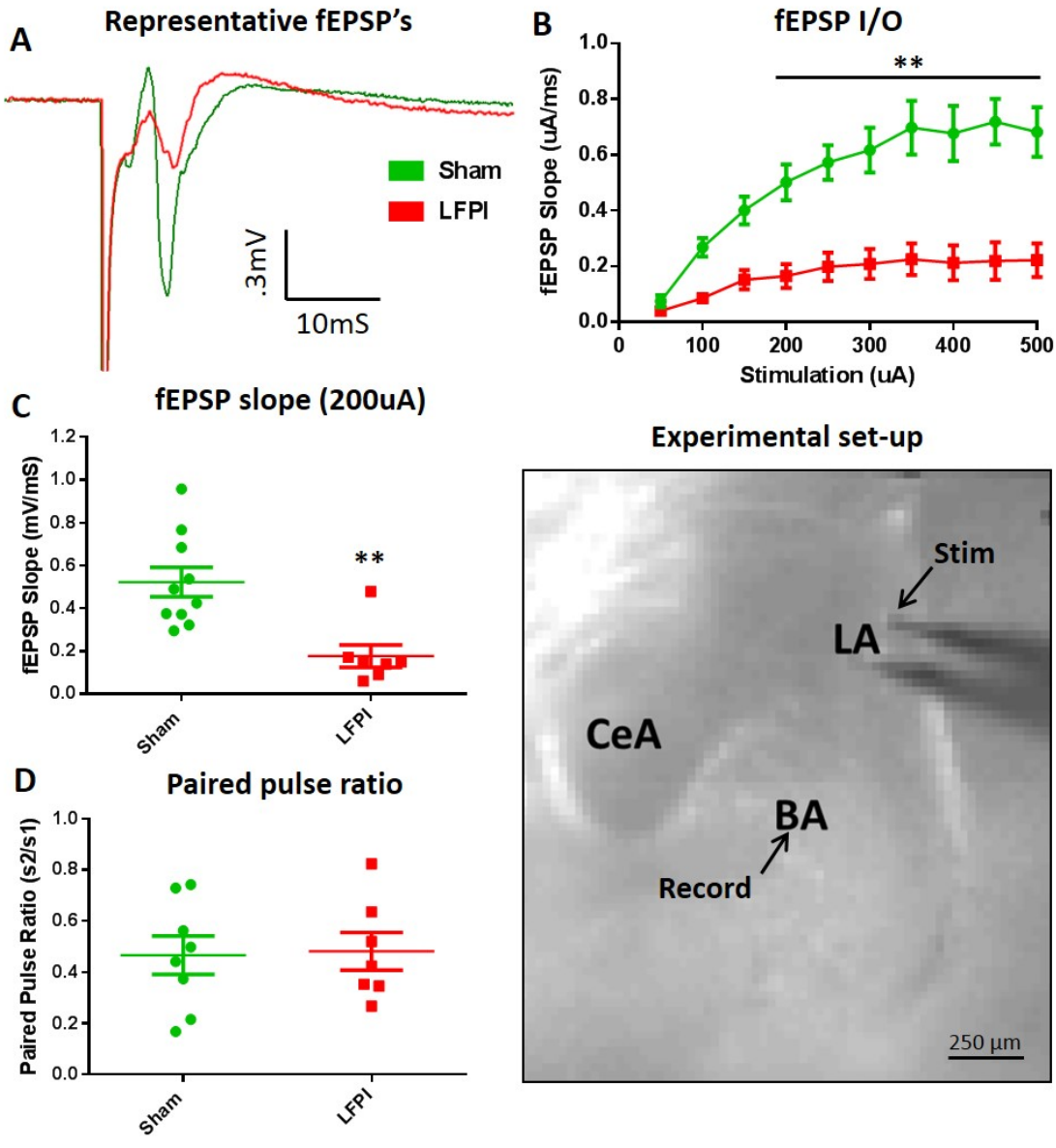
A
Representative fEPSP's
Sham
LFPI
.3mV
10mS
B
fEPSP I/O
**
fEPSP Slope (uA/ms)
Stimulation (uA)
C
fEPSP slope (200uA)
fEPSP Slope (mV/mS)
**
Sham
LFPI
D
Paired pulse ratio
Paired Pulse Ratio (s2/s1)
Sham
LFPI
Experimental set-up
Stim
LA
CeA
BA
Record
250 µm

Figure 3

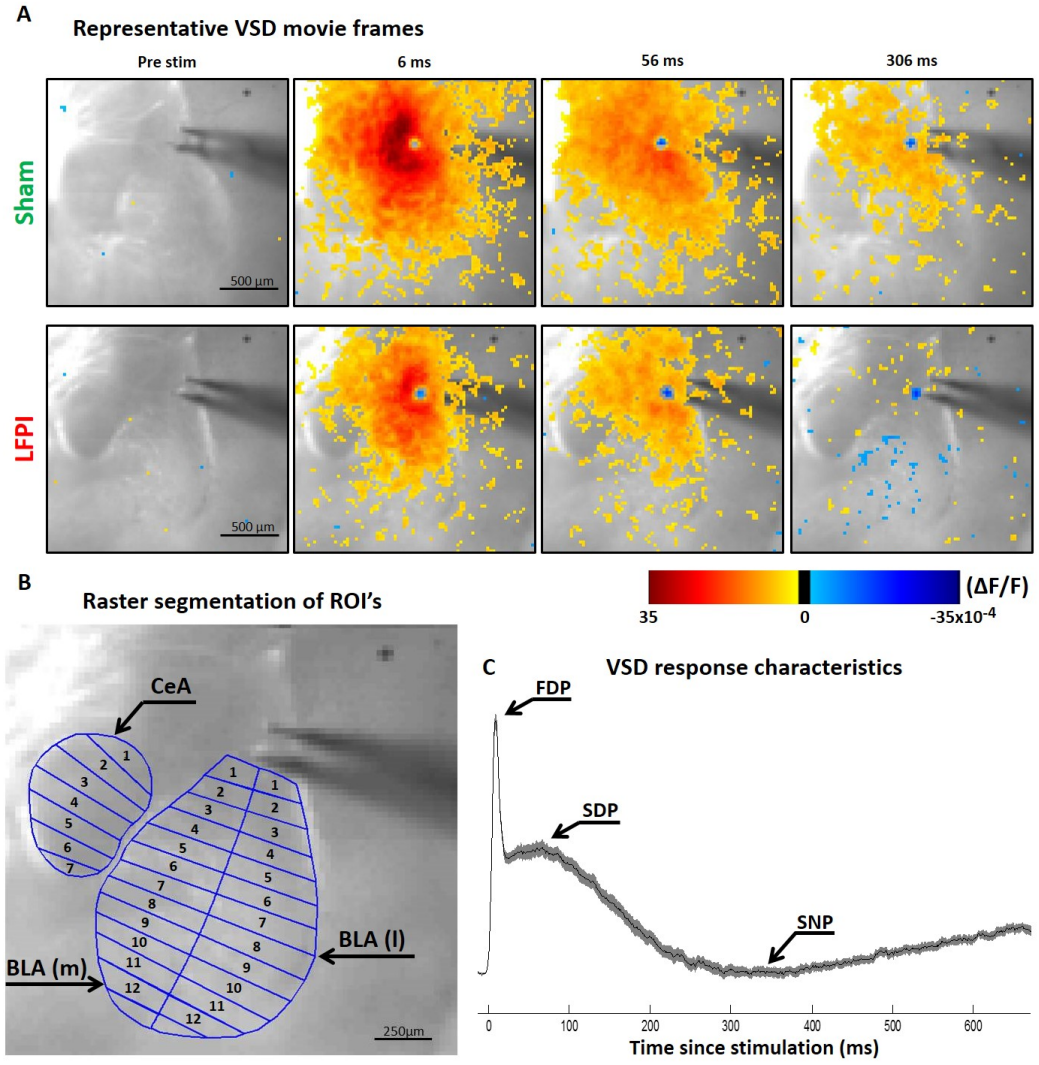
A
Representative VSD movie frames
Pre stim
6 ms
56 ms
306 ms
Sham
LFPI
500 µm
500 µm
B
Raster segmentation of ROI's
(ΔF/F)
35
0
-35x10-4
CeA
BLA (l)
BLA (m)
250µm
C
VSD response characteristics
FDP
SDP
SNP
0
100
200
300
400
500
600
Time since stimulation (ms)

Figure 4

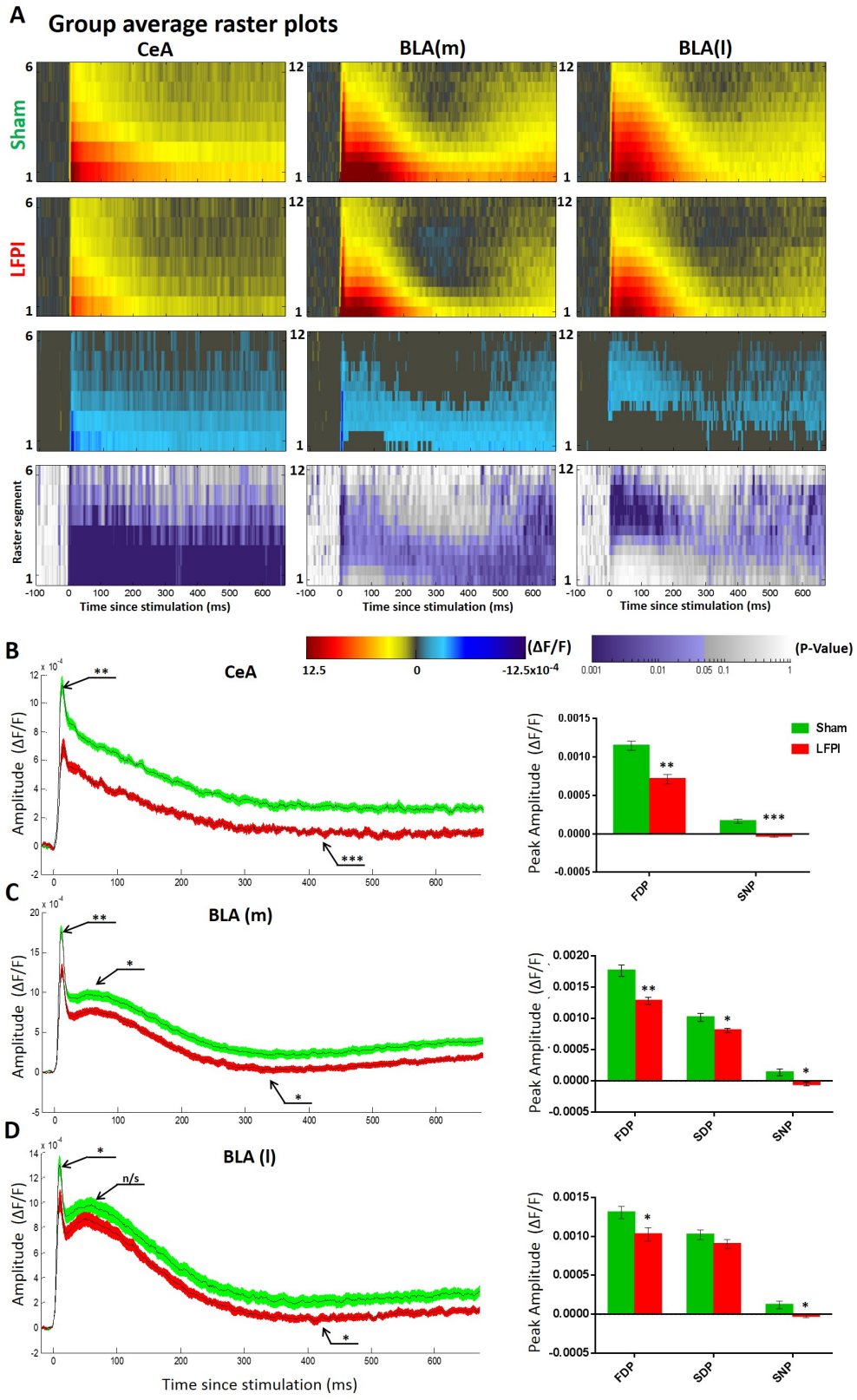
A
Group average raster plots
CeA
BLA(m)
BLA(l)
Sham
LFPI
Raster segment
Time since stimulation (ms)
(ΔF/F)
(P-Value)
B
CeA
C
BLA (m)
D
BLA (l)
Amplitude (ΔF/F)
Peak Amplitude (ΔF/F)
Sham
LFPI
FDP
SDP
SNP
n/s
Time since stimulation (ms)

Figure 5

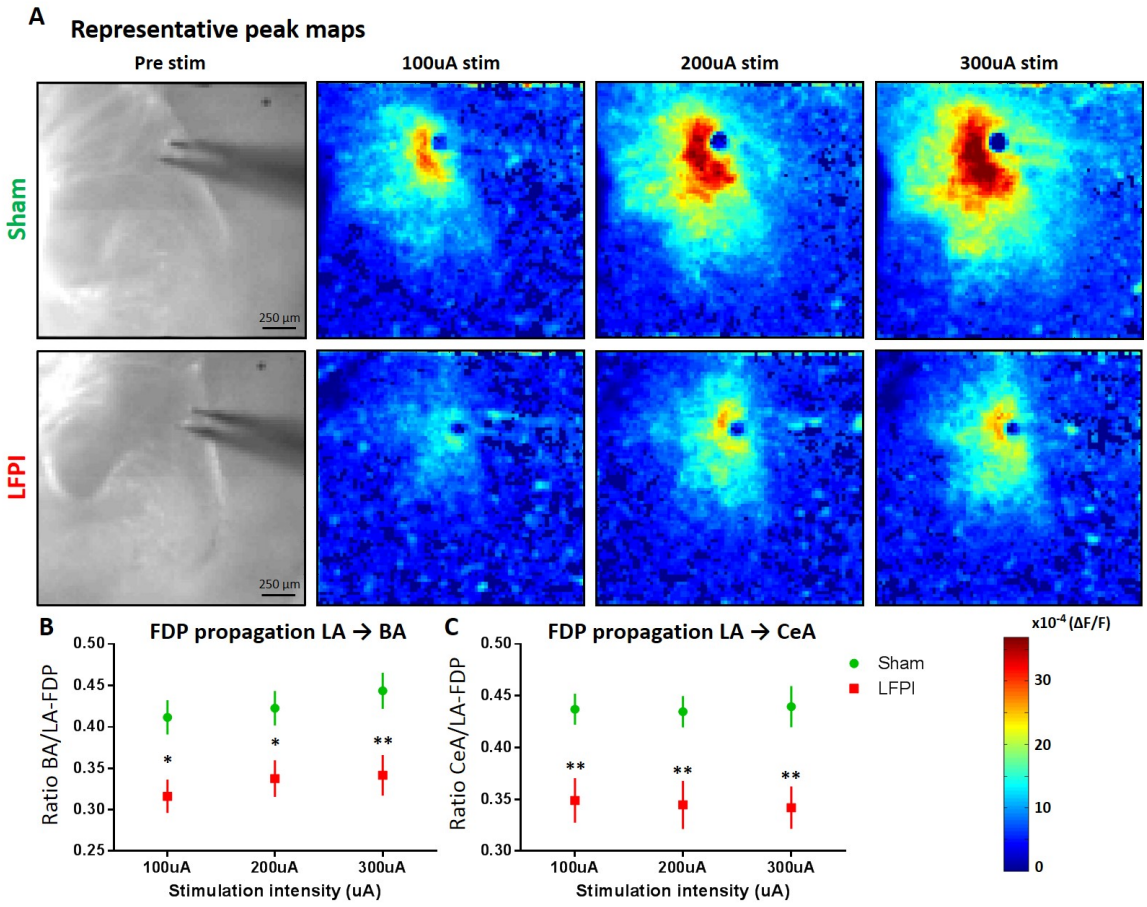
A
Representative peak maps
Pre stim
100uA stim
200uA stim
300uA stim
Sham
LFPI
250 µm
250 µm
B
FDP propagation LA → BA
Ratio BA/LA-FDP
0.50
0.45
0.40
0.35
0.30
0.25
100uA
200uA
300uA
Stimulation intensity (uA)
C
FDP propagation LA → CeA
Ratio CeA/LA-FDP
Sham
LFPI
x10-4 (ΔF/F)
30
20
10
0

Figure 6

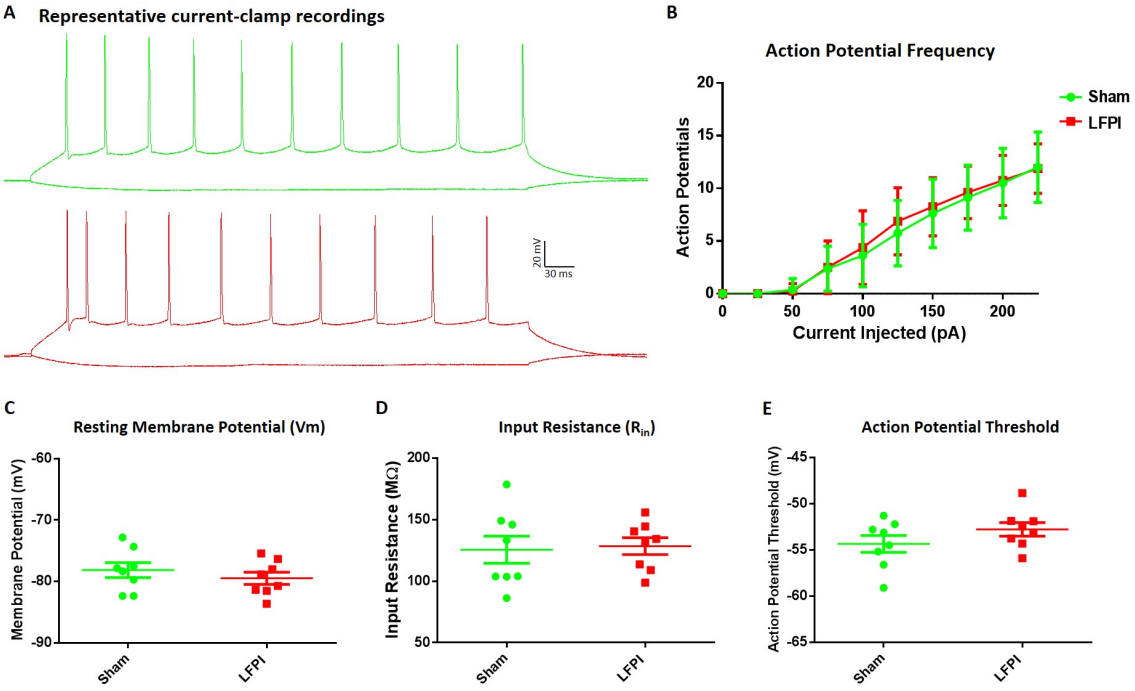
A
Representative current-clamp recordings
20 mV
30 ms
B
Action Potential Frequency
Sham
LFPI
Action Potentials
Current Injected (pA)
C
Resting Membrane Potential (Vm)
Membrane Potential (mV)
D
Input Resistance (R_in)
Input Resistance (MΩ)
E
Action Potential Threshold
Action Potential Threshold (mV)
Sham
LFPI

Figure S1

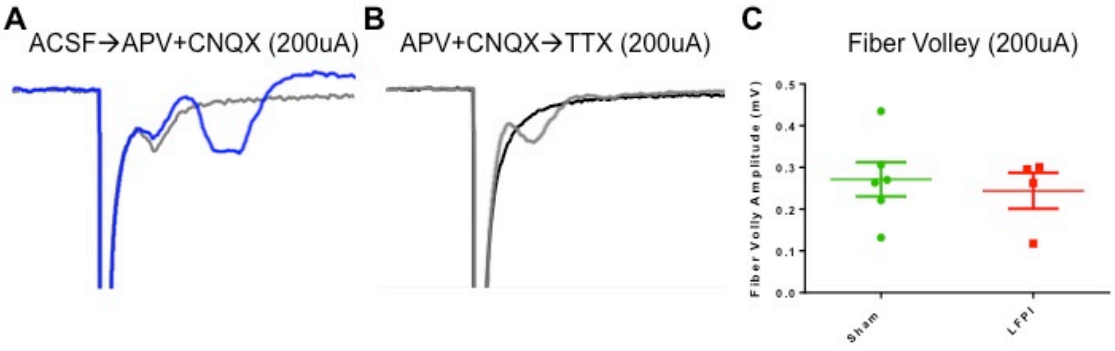
A
ACSF→APV+CNQX (200uA)
B
APV+CNQX→TTX (200uA)
C
Fiber Volley (200uA)
Fiber Volly Amplitude (mV)
0.5
0.4
0.3
0.2
0.1
0.0
Sham
LFPI

Figure S2

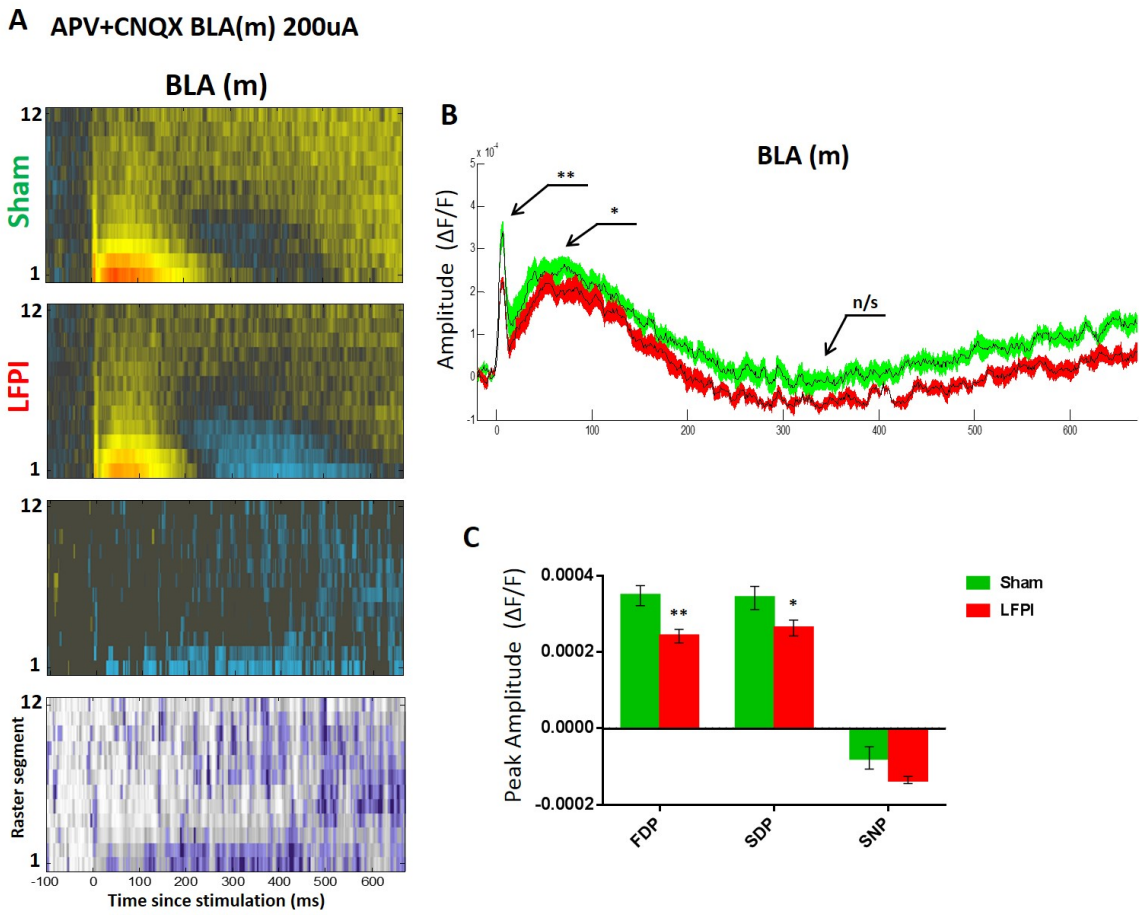
A
APV+CNQX BLA(m) 200uA
BLA (m)
Sham
LFPI
12
1
Raster segment
-100
0
100
200
300
400
500
600
Time since stimulation (ms)
B
BLA (m)
Amplitude (ΔF/F)
**
*
n/s
C
Peak Amplitude (ΔF/F)
0.0004
0.0002
0.0000
-0.0002
FDP
SDP
SNP
Sham
LFPI

Figure S3

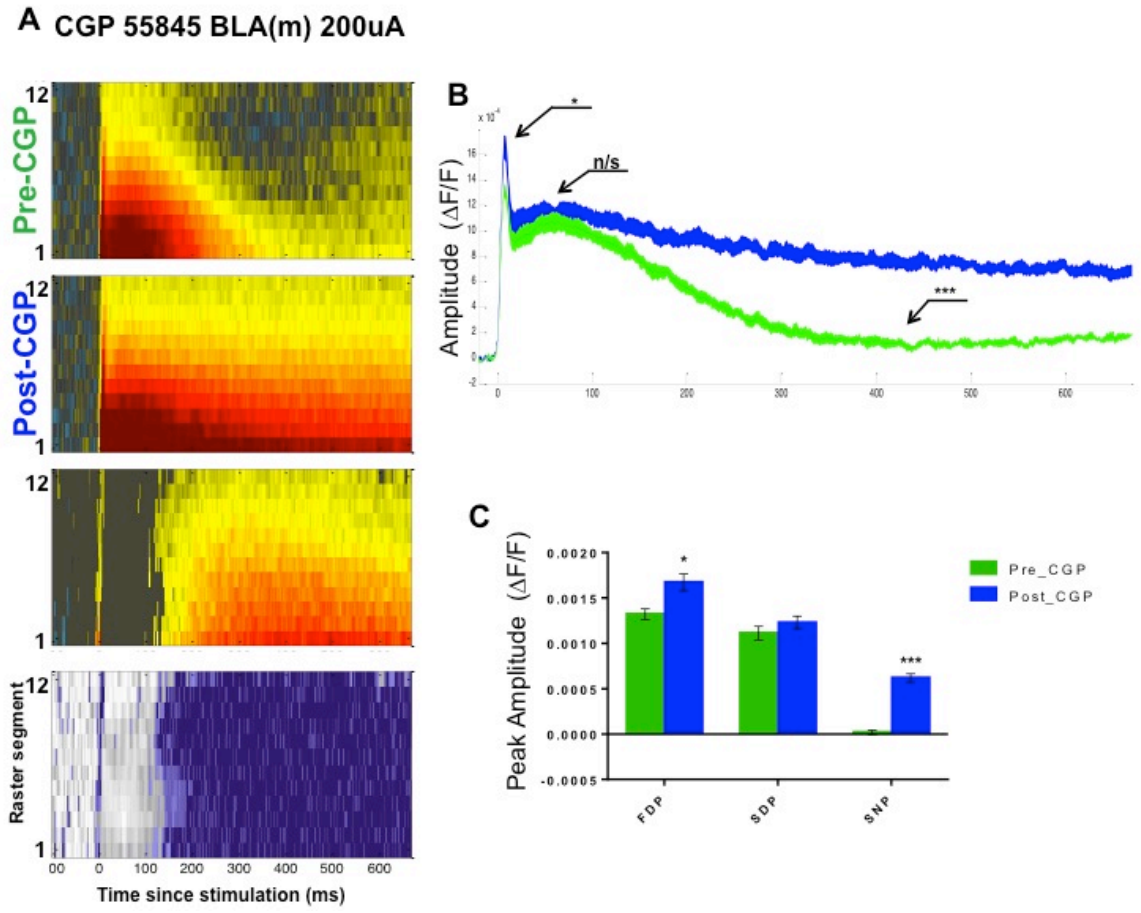
A CGP 55845 BLA(m) 200uA
Pre-CGP
Post-CGP
Raster segment
Time since stimulation (ms)
B
Amplitude (ΔF/F)
n/s
C
Peak Amplitude (ΔF/F)
Pre_CGP
Post_CGP
FDP
SDP
SNP

Video S1

http://proxy.library.upenn.edu:2067/science/article/pii/S0014488616300048

Video S2

http://proxy.library.upenn.edu:2067/science/article/pii/S0014488616300048

CHAPTER 3

Preliminary findings on the mechanism of traumatic brain injury induced decreased network excitability of the basolateral amygdala

Christopher P. Palmer [a], Hannah E. Metheny [b], Akiva S. Cohen [b,c]

[a] Neuroscience Graduate Group and [c] Critical Care Medicine, Department of Anesthesiology, Perelman School of Medicine, University of Pennsylvania: 3451 Walnut Street, Philadelphia, PA 19104

[b] Critical Care Medicine, Department of Anesthesiology, The Children's Hospital of Philadelphia: 3401 Civic Center Blvd, Philadelphia, PA 1910

Abstract:

Individuals that suffer a traumatic brain injury (TBI) are at a heightened risk of developing an array of debilitating neuropsychological symptoms ranging from aggression to depression. Due to its unique role in determining the emotional response to stimuli and assigning emotional valence, dysfunction in the amygdala is often hypothesized to be the neural substrate of the neuropsychological symptoms of TBI. Experiments performed in our laboratory and others have identified circuit level dysfunction in the amygdala following mild to moderate traumatic brain injury (mTBI), concomitant with deficits in amygdala dependent behaviors. While it has been shown that network excitability and connectivity of the amygdala can be altered by mTBI, the mechanism underlying this alteration is poorly understood. Understanding the mechanisms contributing to TBI induced amygdala circuit dysfunction is essential for the potential development of future therapeutics targeted at ameliorating the neuropsychological symptoms of TBI. In order to begin elucidating the mechanism of injury induced alterations to amygdala physiology; we performed a series of whole-cell voltage-clamp recordings of basolateral amygdala pyramidal neurons to assess glutamatergic excitation and GABAergic inhibition onto the principal cell type in the basolateral amygdala (BLA). Results from these preliminary experiments have revealed a decrease in excitatory tone, via suppressed spontaneous and evoked glutamatergic excitatory post synaptic currents; and in increase in the ratio of inhibition to excitation following mTBI. Furthermore, the significant decrease in glutamatergic excitation within the BLA did not correlate to a decrease in polysynaptic GABAergic inhibition; suggesting that polysynaptic inhibition in the BLA is augmented or selectively preserved

after TBI. Taken together these findings suggest opposing shifts in glutamatergic excitation and GABAergic inhibition that both contribute to the decreased network excitability observed in the BLA following mTBI.

Introduction:

Traumatic brain injury is a growing epidemic afflicting millions of Americans each year and is the leading cause of death and disability in children and young adults (Langlois et al., 2006; Rutland-Brown et al., 2006; Faul and Coronado, 2015). Growing rates of hospitalization for TBI coupled with advances in medicine that decreased the mortality rate of TBI, have resulted in an ever-growing population of TBI survivors; many of whom suffer some form of TBI related disability (Zaloshnja et al., 2008; Faul and Coronado, 2015) Neuropsychological symptoms including aggression, anxiety, irritability, rage, poor impulse control, depression, anhedonia, and apathy are among the most common prolonged symptoms reported by TBI survivors (Jorge et al., 2004; Bazarian et al., 2009; Rao et al., 2009; Riggio, 2010; Malkesman et al., 2013). These symptoms contribute to an increase in substance abuse, incarceration, suicidality, and mortality rate among TBI survivors (Langlois et al., 2006).

Due to the array of neuropsychological symptoms seen in TBI patients, dysfunction of the amygdala, a brain region integral in emotional expression (Ledoux, 2000; LeDoux, 2012), is thought to play a role in the acquisition and/or expression of these symptoms. This hypothesis is supported by a number of both human and animal studies that have found brain injury-induced alterations to amygdala anatomy, connectivity and physiology, some specifically in patients suffering neuropsychiatric sequelae after TBI (Juranek et al., 2011; Almeida-Suhett et al., 2014; Depue et al., 2014; Han et al., 2015; Klein et al., 2015; Palmer et al., 2016). Previous work form our laboratory using a mouse model of mild to moderate traumatic brain injury (mTBI)

demonstrated an injury-induced decrease in network excitability and internuclear circuit strength in the amygdala, associated with deficits in amygdala dependent behaviors (Palmer et al., 2016). While the aforementioned study reveals brain injury-induced circuit level dysfunction in amygdalar physiology following TBI, the mechanism underlying this physiological dysfunction is yet unknown. In this study we employ single cell electrophysiological techniques to begin determining the mechanism of the observed decrease in amygdalar network excitability following TBI.

Using a well-established mouse model of mild to moderate traumatic brain injury, lateral fluid percussion injury (LFPI); we performed a series of whole-cell voltage-clamp recordings of basolateral amygdala pyramidal neurons to assess glutamatergic excitation and GABAergic inhibition onto the principal cell type in the basolateral amygdala (BLA), following TBI. We began by recording spontaneous excitatory post synaptic currents (sEPSCs) in cells from brain slices of sham and LFPI animals, to assess excitatory drive. We then delivered a series of electrical stimulations to the primary input region of the BLA, the lateral amygdala (LA), while injecting current to hold the recorded neuron at the reversal potential initially for AMPA/glutamate receptors and subsequently for $GABA_A$ receptors; allowing us to electrically isolate and record glutamatergic and GABAergic currents independently in the same cell. The neurotransmitter receptors generating each current were also confirmed pharmacologically. The results of these experiments demonstrate an LFPI-induced decrease in glutamatergic neurotransmission and suggest an opposing augmentation of glutamate dependent polysynaptic GABAergic inhibition. Overall, at the level of a single

cell this results in an increase in the ratio of inhibition to excitation onto BLA pyramidal neurons following brain injury.

Materials and Methods:

Animals

All experiments were performed on 7 to 12 week-old, male C57BL/J6 mice (The Jackson Laboratory). All animals were group housed with free access to food and water. All procedures were performed in accordance with the guidelines published in the National Institutes of Health (NIH) Guide for the Care and Use of Laboratory Animals and approved by the Children's Hospital of Philadelphia Institutional Animal Care and Use Committee.

Lateral Fluid Percussion Injury

Lateral fluid percussion injury (LFPI) is an established model of mild to moderate traumatic brain injury that mimics many aspects of human TBI pathology and symptomatology validated by decades of use (Carbonell et al., 1998; Thompson et al., 2005; Xiong et al., 2013). LFPI procedure was performed as previously described in (Palmer et al., 2016). Briefly, animals were assigned into one of three groups; Naïve animals that received no surgery or injury, but were treated otherwise identically; LFPI (surgery+injury); or sham (surgery only). Surgery and injury were performed on consecutive days, for full details see (Witgen et al., 2005; Cole et al., 2010). On day one mice were anesthetized with a combination of ketamine (100 mg/kg) and xylazine (10 mg/kg) and placed in a stereotaxic frame (Stoelting). A 3 mm outer diameter trephine was then used to perform a craniectomy of the right parietal bone lateral of the sagittal suture between lambda and bregma, without disrupting the intact dura. A Luer-loc needle

hub (3 mm inner diameter) was secured to the skull surrounding the craniectomy with adhesive and dental cement. The needle hub was filled with sterile saline solution and sealed overnight. On the following day, LFPI animals were anesthetized with isoflurane and connected to the LFPI device (Department of Biomedical Engineering, Virginia Commonwealth University, Richmond, VA). The LFPI device was then triggered, delivering a 10-15 ms fluid pulse (peak pressure 1.5-1.8 atm) onto the intact dura of the brain to generate a mild to moderate TBI. The needle hub was removed and the incision sutured. Any animals with injuries resulting in dural breach or herniation were excluded from the study. Sham animals underwent an identical procedure without receiving the fluid pulse injury. Results from sham and naïve animals were pooled for analysis and referred to as the sham group.

Electrophysiology

All electrophysiological experiments were performed on days 6-8 after injury or sham surgery. Slice preparation was performed as previously described (Johnson et al., 2014; Palmer et al., 2016). Briefly, animals were anesthetized with isoflurane, the brain was dissected out and placed in ice-cold oxygenated (95%O_2 / 5%CO_2) sucrose-containing artificial cerebrospinal fluid (aCSF) containing (in mM): sucrose 202, KCl 3, NaH_2PO_4 2.5, $NaHCO_3$ 26, glucose 10, $MgCl_2$ 1, $CaCl_2$ 2. Coronal slices 300 μm thick were cut on a vibratome (VT1200S, Leica Microsystems, Buffalo Grove, IL, USA) and transferred to 33–37°C oxygenated (95%O_2 / 5%CO_2) control aCSF containing (in millimolar): NaCl 130, KCl 3, NaH_2PO_4 1.25, $NaHCO_3$ 26, glucose 10, $MgCl_2$ 1, $CaCl_2$ 2. Slices were allowed to incubate for at least 60 min before recording. Intracellular

whole-cell voltage-clamp recordings were performed in a submersion chamber with a flow rate of approximately 2.0 ml/min and maintained at 33°C. Brain slices for recording were consistently selected from the same rostral-caudal region of the amygdala that exhibited a pear shaped basolateral amygdala (BLA) contiguous with an ovoid central amygdala (CeA). This rigid criterion resulted in 1-2 brain slices per animal. Brain slices were hemisected prior to recording and only slices from the hemisphere ipsilateral to the site of injury were used. Our laboratory has previously demonstrated that contralateral slices are altered by LFPI and thus do not serve as an appropriate control for the injured hemisphere (Tran et al., 2006). A maximum of 1 cell per brain slice was used for analysis. An effort was made to patch cells from the central portion of the BLA, near where the field electrode was placed in the experiments described in (Palmer et al., 2016). However, as visualized patch-clamp experiments are performed under higher magnification (63x) and cells must meet certain anatomical criteria, the spatial locations of neurons recorded is more varied in this set of experiments than the prior field recordings.

Whole-cell voltage-clamp recording electrodes were fabricated from borosilicate glass (World Precision Instruments, Sarasota, FL, USA, #1B150F-4) pulled to a tip resistance of 4–7 MΩ and filled with an internal solution containing (in milimolar): KGluconate 145, KCl 2.5, NaCl 2.5, HEPES 10, $MgCl_2$ 2, ATP.Mg 2, GTP.Tris 0.5, and BAPTA .1. Internal solutions for experiments recording lateral amygdala stimulation evoked currents also contained (in millimolar): Lidocaine N-ethyl bromide (QX314) 5, to antagonize voltage-gated sodium channels, thereby suppressing action potential

generation and isolating synaptic currents. Whole-cell recordings of BLA pyramidal neurons were performed using a Multiclamp 700B amplifier and pClamp10 data acquisition software (Molecular Devices, Sunnyvale, CA, USA). All recording voltages were corrected for a liquid junction potential calculated at −14.5 mV (using the Junction Potential utility in Clampex 10.3), and a series voltage error of 2.2 mV. Current was injected to bring cells to the target holding/resting membrane potential for the given experiment. Target membrane potential values were chosen to isolate either glutamatergic or GABAergic currents by holding at the calculated reversal potential for the other. The calculated reversal potentials were ($GABA_A$ = -72.4mV) and (AMPA = .7mV). Only recordings with a series resistance of less than 25 MΩ were used in analysis. Series resistance was compensated at 75%. BLA pyramidal neurons were identified on the basis of previously characterized morphological and physiological properties (Sah et al., 2003). Addition of Lidocaine N-ethyl bromide (QX314) in a subset of experiments does preclude physiological identification of fast spiking interneurons that comprise approximately 7% of neurons in the BLA. Thus, it is possible that the putative BLA pyramidal cell population used for evoked current recordings is contaminated by fast spiking interneurons by less than or equal to 7%. Whole-cell voltage-clamp data was analyzed using pClamp10 software.

Spontaneous excitatory post synaptic currents (sEPSCs) were recorded in 5 min epochs while holding at the calculated $GABA_A$ reversal potential (-72.4 mV). No stimulation was delivered during sEPSC recordings. Recorded sEPSCs were visually sorted and analyzed for frequency and amplitude. sEPSCs were completely suppressed by

bath application of 50 μM D-(-)-2-Amino-5-phosphonopentanoic acid (APV) + 6 μM 6-Cyano-7-nitroquinoxaline-2,3-dione (CNQX) to suppress ionotropic glutamatergic transmission (**Fig. 1**).

In a subset of cells lateral amygdala stimulation evoked currents were recorded immediately following sEPSC recordings. Stimulating electrodes were non-concentric bipolar (World Precision Instruments, Sarasota, FL, USA, #ME12206) and placed in the dorsal most portion of the lateral amygdala (LA), just medial of the external capsule. Electrical stimuli were 100 μs in duration. Evoked excitatory and inhibitory post synaptic current (eEPSC & eIPSC) input-output relationships (50-350 μA stim, 50 μA increments, 8 s inter stimulus interval) were both recorded in each cell to allow comparison between inhibition and excitation within a given cell. eEPSCs were recorded at the calculated $GABA_A$ reversal potential (-72.4 mV) and completely suppressed by bath application of 50 μM D-(-)-2-Amino-5-phosphonopentanoic acid (APV) + 6 μM 6-Cyano-7-nitroquinoxaline-2,3-dione (CNQX) (**Fig. 4**). To record eIPSCs, cells were very briefly held at the calculated $GABA_A$ reversal potential (.7 mV). To minimize the time that the cell was held at this depolarized membrane potential and in attempt to prevent depolarization induced suppression of inhibition; LA stimulation occurred shortly after the leak currents activated by this voltage step stabilized (≈200 ms) and the cell was maintained at this membrane potential for only 300 ms post stimulus while the eIPSC was recorded. eIPSCs were completely suppressed by bath application of bicuculline methiodide (30 μM) to suppress $GABA_A$ currents (**Fig. 6**). A subset of eIPSCs were also recorded in the presence of 50 μM D-(-)-2-Amino-5-phosphonopentanoic acid (APV) + 6

μM 6-Cyano-7-nitroquinoxaline-2,3-dione (CNQX) to calculate the polysynaptic component of the eIPSC (**Fig. 8**). eEPSCs and eIPSCs were analyzed for peak amplitude and area (eIPSC: first 185ms after onset of response ; eEPSC: first 55ms after onset of response). To calculate the ratio of inhibition to excitation within cells we divided the peak amplitude or area of the eIPSC by the peak amplitude or area of the eEPSC for a given stimulation intensity.

Statistical Procedures

All statistical analyses and calculations were performed using GraphPad Prism. All statistical tests for significance were conducted using Mann-Whitney U-tests or two-way repeated-measures ANOVA with Sidak's multiple comparison test in order to test for injury effect and stimulation intensity effect. Statistical significance was $P < 0.05$ ($P < 0.05$*, $P < 0.01$**, $P < 0.001$***). N values are reported per cell and per animal with a maximum of 1 cell per brain slice and 2 slices per animal. Data in the figures are presented as group means ± SEM.

Results:

LFPI causes a decrease in the frequency of spontaneous excitatory post synaptic currents onto basolateral amygdala pyramidal neurons

To begin characterizing the mechanism underlying the brain injury-induced alterations in network excitability and circuit strength of the basolateral amygdala shown in (Palmer et al., 2016), we performed a series of whole-cell voltage-clamp recordings of spontaneous excitatory post synaptic currents (sEPSCs) in BLA pyramidal neurons. Previous reports from our laboratory and others have shown changes in spontaneous synaptic activity correlating with altered network excitability across multiple brain regions after TBI (Witgen et al., 2005; Almeida-Suhett et al., 2014; Klein et al., 2015; Smith et al., 2015). Thus, if there is a change in the excitatory tone of the BLA this could manifest as a change in frequency or amplitude of sEPSCs.

Cells were held at the reversal potential for GABAergic ($GABA_A$) transmission, (-72.4mV), to eliminate inhibitory currents and isolate spontaneous excitatory currents. The remaining spontaneous currents were depolarizing and completely abolished by bath application of glutamatergic antagonists 50 μM D-(-)-2-Amino-5-phosphonopentanoic acid (APV) + 6 μM 6-Cyano-7-nitroquinoxaline-2,3-dione (CNQX) (**Fig. 1**); ensuring they were indeed glutamatergic sEPSCs. LFPI caused a significant decrease in the frequency of sEPSCs onto BLA pyramidial neurons (**Fig. 2B,** sham = 6.43, 95% CI 5.17-11.1 Hz, n=11 cells 10 animals; LFPI = 4.38 %, 95% CI 3.44-5.60 Hz n=11 cells 8

animals; *P* =0.034) with no change in peak amplitude (**Fig. 2C,** sham = 29.0, 95% CI 27.1-33.1 Hz, n=11 cells 10; LFPI = 28.4, 95% CI 24.3-33.5 Hz n=11 cells 8 animals; *P* =0.55).

LFPI causes opposing shifts in lateral amygdala stimulation evoked glutamatergic excitation and GABAergic inhibition onto basolateral amygdala pyramidal neurons

As the results from the previous experiments demonstrate an LFPI-induced decrease in excitatory tone and spontaneous glutamatergic transmission, we next sought to confirm this decrease in glutamatergic excitation and directly compare glutamatergic excitation to GABAergic inhibition within the same BLA pyramidal neurons. To accomplish this we performed a series of voltage-clamp recordings of electrically isolated LA stimulation evoked glutamatergic excitation, or evoked excitatory post synaptic currents (eEPSCs), and LA stimulation evoked GABAergic inhibition, or evoked inhibitory post synaptic currents (eIPSCs), within the same cell. 5 mM Lidocaine N-ethyl bromide (QX314) was included in the internal solution for these experiments to prevent action potential firing from contaminating eEPSCs & eIPSCs.

As previously described, eEPSCs were recorded while holding the recorded neuron at the calculated reversal potential for $GABA_A$ mediated currents. Representative eEPSC responses to increasing stimulation intensities in cells from brain slices of sham

and LFPI animals can be seen in (**Fig. 3A**). As indicated by the representative recordings, LFPI causes a significant decrease in the amplitude (**Fig. 3B,** sham n=10 cells 7 animals, LFPI n=9 cells 7 animals, two-way repeated-measures ANOVA, (injury effect) F (1,17) = 6.086 ; P = 0.025) and area (**Fig. 3C,** sham n=10 cells 7 animals, LFPI n=9 cells 7 animals, two-way repeated-measures ANOVA, (injury effect) F (1,17) = 10.10 ; P = 0.006) of LA stimulation eEPSCs onto BLA pyramidal neurons. eEPSCs were blocked by bath application of NMDA and AMPA receptor antagonists 50 μM D-(-)-2-Amino-5-phosphonopentanoic acid (APV) + 6 μM 6-Cyano-7-nitroquinoxaline-2,3-dione (CNQX) (**Fig. 4**).

eIPSCs were recorded while holding the recorded neuron at the calculated reversal potential for AMPA glutamate receptors (.7mV). Representative eIPSC responses to increasing stimulation intensities in cells from brain slices of sham and LFPI animals can be seen in (**Fig. 5A**). Depolarized holding potentials were kept intentionally brief to preserve cell health and prevent excessive depolarization induced suppression of inhibition (see methods for full details). As indicated by the representative recordings, LFPI causes no change in the amplitude (**Fig. 5B,** sham n=10 cells 7 animals, LFPI n=9 cells 7 animals, two-way repeated-measures ANOVA, (injury effect) F (1,17) = 0.001 ; P = 0.978) or area (**Fig. 5B,** sham n=10 cells 7 animals, LFPI n=9 cells 7 animals, two-way repeated-measures ANOVA, (injury effect) F (1,17) = 0.301 ; P = 0.585) of LA stimulation eIPSCs onto BLA pyramidal neurons. eIPSCs were blocked by bath application of the $GABA_A$ antagonist 30 μM bicuculline methiodide (BMI) (**Fig. 6**). The prolonged depolarizing current seen in the presence of BMI could represent the unveiling

of an unanticipated synaptic current; alternatively, the authors hypothesize that this depolarization is rather a homeostatic response to the increase in extracellular potassium caused by the excessive action potential generation likely present in the BLA when $GABA_A$ receptors are antagonized.

We next compared the amount of GABAregic inhibition to glutamatergic excitation within cells to determine if the proportion of inhibition relative to excitation was altered by LFPI. Recording these measures within the same cell gives us a more complete picture of synaptic inputs onto BLA neurons and allows us to more accurately quantify the balance of excitation and inhibition at a cellular level. In order to quantify this balance, we created a ratio of inhibition to excitation within cells by dividing the peak amplitude or area of the eIPSC by the peak amplitude or area of the eEPSC for the corresponding stimulation intensity. LFPI caused a significant increase in the ratio of inhibition to excitation as measured by amplitude (**Fig. 7A,** sham n=10 cells 7 animals, LFPI n=9 cells 7 animals, two-way repeated-measures ANOVA, (injury effect) F (1,17) = 10.83 ; P = 0.004) and area (**Fig. 7B,** sham n=10 cells 7 animals, LFPI n=9 cells 7 animals, two-way repeated-measures ANOVA, (injury effect) F (1,17) = 5.68 ; P = 0.029), demonstrating a shift in the inhibition/excitation balance following LFPI.

While most of the aforementioned results could be attributed to a decrease in excitatory drive or a general depression of synaptic function, the fact that inhibition is unaltered despite a decrease in excitation suggests the inhibitory system is also affected by LFPI. Inhibitory interneurons comprise approximately 20% of neurons within the

basolateral amygdala, many of which synapse perisomatically on BLA pyramidal neurons and participate in feedforward/feedback inhibition (Rainnie et al., 1991; Sah et al., 2003; Duvarci and Pare, 2014; Wolff et al., 2014; Prager et al., 2015). If the eIPSC recorded in our above experiments is indeed largely polysynaptic and activated by glutamatergic transmission, we would hypothesize the eIPSC to be significantly suppressed as a result of the decrease in glutamatergic excitation. To assess the glutamate dependent polysynaptic component of the eIPSC, we compared the eIPSC amplitude pre and post bath application of 50 μM D-(-)-2-Amino-5-phosphonopentanoic acid (APV) + 6 μM 6-Cyano-7-nitroquinoxaline-2,3-dione (CNQX). This suppression of glutamatergic transmission caused an average 94% decrease in eIPSC amplitude across all stimulation intensities in all cells tested (**Fig. 8**), (200uA stimulation intensity: eIPSC amplitude pre APV+CNQX = 3450 ± 897pA, eIPSC amplitude post APV+CNQX 211 ± 210pA, n=3 cells from 3 animals), confirming the eIPSC is polysynaptic and dependent upon glutamatergic activation.

Discussion:

The amygdala is an integral part of human emotional responses and has been directly linked to several neuropsychological symptoms of traumatic brain injury (Ledoux, 2000; Phelps and LeDoux, 2005; Han et al., 2015). Further, the survival circuits and functions involving the amygdala that we study in animal models most likely correlate and contribute, if indirectly, to the higher order emotional responses and conscious feelings of humans (Phelps and LeDoux, 2005; LeDoux, 2012). In this study we take another step toward understanding the complexities of synaptic and circuit level dysfunction in the amygdalae of animals that have sustained a traumatic brain injury. Building upon the results of our previous study demonstrating circuit level dysfunction in the amygdala associated with an altered behavioral threat response following LFPI (Palmer et al., 2016); in this study we began to characterize the mechanism of physiological alterations in the amygdala of brain injured animals using a series of whole-cell voltage-clamp recordings in basolateral amygdala (BLA) pyramidal neurons. First, we recorded spontaneous excitatory post synaptic currents (sEPSCs) onto BLA pyramidal neurons from brain slices of sham and LFPI animals, demonstrating a significant decrease in the frequency of sEPSCs following LFPI. Next, we recorded lateral amygdala (LA) stimulation evoked excitatory and inhibitory post synaptic currents (eEPSCs & eIPSCs) onto BLA pyramidal neurons, to quantify the balance of glutamatergic and GABAergic currents within the BLA. These experiments demonstrated a brain injury-induced increase in the ratio of inhibition to excitation, at least partially caused by a decrease in glutamatergic excitation that did not coincide with a decrease in glutamate dependent polysynaptic inhibition. Taken together these results suggest that

LFPI has opposing effects on the glutamatergic and GABAergic neurotransmitter systems, resulting in a disruption of the balance of excitation and inhibition within the BLA.

Recording and analysis of spontaneous synaptic currents is common first step towards understanding the mechanism of network dysfunction in the field of traumatic brain injury, and often reveals injury-induced alterations that help to identify the source of physiological perturbations (Santhakumar et al., 2002; Witgen et al., 2005; Gupta et al., 2012; Almeida-Suhett et al., 2014; Klein et al., 2015; Smith et al., 2015). Therefore, to assess excitatory synaptic drive in the BLA we began by recording glutamatergic sEPSCs in the principal cell type of the BLA. These experiments revealed a significant decrease in the frequency but no change in the amplitude of sEPSCs following LFPI (**Fig. 2**). The decrease in exclusively sEPSC frequency reveals a decrease in excitatory drive and suggests that this alteration has a presynaptic locus. It is possible that cells synapsing onto BLA pyramidal neurons generate fewer spontaneous action potentials or exhibit a decrease in the probability of vesicular release following LFPI. Further, based on the variability of the sham frequencies (**Fig. 2A**) and the heterogeneity of inputs onto specific populations of BLA pyramidal neurons, it is possible that the 3 sham cells displaying the highest frequency sEPSCs receive a shared input that has a high spontaneous firing rate or probability of release; and that this input may be selectively suppressed or damaged by brain injury.

As spontaneous and evoked currents utilize different vesicular pools (Fredj and Burrone, 2009) we recorded eEPSCs & eIPSCs to confirm that this decrease in glutamatergic excitation is present using the same stimulation protocol as (Palmer et al., 2016), and to directly compare glutamatergic excitation to GABAergic inhibition within the same BLA pyramidal neurons. These experiments did indeed reveal a decrease in the amplitude and area of eEPSCs in cells from brain slices of LFPI animals (**Fig. 3**); confirming that evoked glutamatergic currents are diminished by LFPI and likely contribute to the diminished amygdala activation reported in the previous chapter of this thesis. Interestingly, GABAergic eIPSC amplitude and area were unaltered by LFPI (**Fig. 5**), despite a significant decrease in excitatory glutamatergic drive.

Based on the known inhibitory circuitry of the BLA this is surprising, as we would hypothesize that majority of the recorded eIPSC should be the result of feedforward/feedback inhibition from local inhibitory interneurons. Therefore, all else being equal, we would expect a decrease in net excitatory drive in the BLA to decrease the magnitude of polysynaptic inhibition. As this did not occur, we first sought to verify that the majority of the currents comprising the recorded eIPSC were indeed polysynaptic and dependent on activation by glutamatergic transmission (i.e. feedforward or feedback inhibition). We found that bath application of the glutamatergic antagonists APV & CNQX, decreased the amplitude of eIPSCs by an average of 94% across all stimulation intensities and experimental conditions **(Fig. 8)**. The finding that the eIPSC is almost entirely dependent on glutamatergic transmission, yet not diminished by an injury-

induced suppression of glutamatergic excitation, strongly suggests that LFPI is affecting inhibitory neurotransmission in addition to suppressing excitatory neurotransmission.

While further experiments will be required to confirm this preliminary finding and identify the source of preserved or augmented inhibition, the authors can speculate on a few plausible explanations. A simplified BLA circuit diagram was included to aid in explanation of these hypotheses (**Fig. 9**). First, it is possible that excitatory synapses onto local inhibitory interneurons in the BLA (**Fig. 9B**) are selectively spared or augmented by LFPI; such that the decrease present in glutamatergic transmission onto excitatory pyramidal cells (**Fig. 9A**) is missing or compensated at the synapses onto inhibitory interneurons. Next, a single or multiple classes of local inhibitory interneurons could be intrinsically more excitable after LFPI; thereby compensating for the putative decrease in excitatory drive and maintaining a similar output. A cell type specific theory is supported by previous studies that have identified cell type specific alterations in the hippocampus after TBI (Gupta et al., 2012; Johnson et al., 2012). Finally, LFPI could have a direct effect on the pre or post synaptic function of inhibitory synapses onto BLA pyramidal neurons (**Fig. 9C**). Presynaptically, inhibitory currents could be augmented by an increase in probability of vesicular release or up regulation of neurotransmitter packaging into vesicles. Postsynaptically, the same could be accomplished by increasing the density of $GABA_A$ receptors.

With all of the aforementioned results being based on population measures and statistical comparison of values generated across cells; we wanted to look more closely at

how these overall changes affect the balance of inhibition and excitation within individual cells. We examined this by quantifying the ratio of evoked inhibition to excitation within a given cell. Based on the group data we hypothesized and found that the ratio of inhibition to excitation onto BLA pyramidal neurons was significantly augmented by LFPI. Thus, within and across cells, a given amount of excitation is correlated with proportionally more inhibition following LFPI. This increase in the cellular ratio of inhibition to excitation provides a mechanism for the decrease in BLA excitability and circuit strength previously demonstrated in (Palmer et al., 2016).

Figure Legends:

Fig. 1 sEPSCs are blocked by bath application of APV and CNQX. (A) Representative sEPSC recordings from the same BLA pyramidal neuron in standard aCSF (blue) and **(B)** aCSF containing 50 μM APV + 6 μM CNQX (black), demonstrating that sEPSCs are glutamatergic. Current was injected to maintain the membrane potential at approximately -72.4 mV.

Fig. 2 sEPSC frequency onto BLA pyramidal neurons is decreased following LFPI. **(A)** Representative sEPSC recordings from BLA pyramidal neurons from brain slices from sham (green) and LFPI (red) animals. **(B)** Graph of frequency of sEPSCs in cells from sham and injured animals, showing a significant reduction in LFPI animals. **(C)** Graph of amplitude of sEPSCs in cells from sham and injured animals, showing no change in LFPI animals. Current was injected to maintain the membrane potential at approximately -72.4 mV.

Fig. 3 Lateral amygdala stimulation eEPSCs onto BLA pyramidal neurons are decreased following LFPI. (A) Representative eEPSC recordings from BLA pyramidal neurons from brain slices from sham (green) and LFPI (red) animals. **(B)** Graph of peak amplitudes of eEPSCs in cells from sham and injured animals, showing a significant reduction in LFPI animals. **(C)** Graph of areas of eEPSCs in cells from sham and injured animals, showing a significant reduction in LFPI animals. Current was injected to maintain the membrane potential at approximately -72.4 mV.

Fig. 4 Lateral amygdala stimulation eEPSCs are blocked by bath application of APV and CNQX. (A) Representative lateral amygdala stimulation (50-450 μA, 50 μA steps, stimulation) eEPSC recordings from the same BLA pyramidal neuron in standard aCSF (blue) and **(B)** aCSF containing 50 μM APV + 6 μM CNQX (black), demonstrating that eEPSCs are glutamatergic. Current was injected to maintain the membrane potential at approximately -72.4 mV.

Fig. 5 Lateral amygdala stimulation eIPSCs onto BLA pyramidal neurons are unaffected by LFPI. (A) Representative eEPSC recordings from BLA pyramidal neurons from brain slices from sham (green) and LFPI (red) animals. **(B)** Graph of peak amplitudes of eIPSCs in cells from sham and injured animals, showing no affect of LFPI. **(C)** Graph of areas of eIPSCs in cells from sham and injured animals, showing no affect of LFPI. Current was injected to maintain the membrane potential at approximately .7 mV.

Fig. 6 Lateral amygdala stimulation eIPSCs are blocked by bath application of bicuculline methiodide (BMI). (A) Representative lateral amygdala stimulation (50-350 μA, 50 μA steps, stimulation) eIPSC recordings from the same BLA pyramidal neuron in standard aCSF (blue) and **(B)** aCSF containing 30 μM bicuculline methiodide (black), demonstrating that eIPSCs are mediated via $GABA_A$ receptors. Current was injected to maintain the membrane potential at approximately .7 mV.

Fig. 7 Intra cell lateral amygdala stimulation eIPSC/eEPSC ratio is significantly augmented following LFPI. (A) Graph of intra cell eIPSC/eEPSC peak amplitude ratios in cells from sham and injured animals, showing a significant increase following LFPI. **(B)** Graph of intra cell eIPSC/eEPSC area ratios in cells from sham and injured animals, showing a significant increase following LFPI.

Fig. 8 Lateral amygdala stimulation eIPSCs are largely abolished by application of APV and CXQX. (A) Representative lateral amygdala stimulation (50-350 μA, 50 μA steps, stimulation) eIPSC recordings from the same BLA pyramidal neuron in standard aCSF (blue) and **(B)** aCSF containing 50 μM APV + 6 μM CNQX (black), demonstrating that eIPSCs are polysynaptic and dependant upon glutamatergic transmission. Current was injected to maintain the membrane potential at approximately .7 mV.

Fig. 9 Simplified basolateral amygdala circuit schematic. Circuit diagram showing excitatory and inhibitory synapses onto BLA pyramidal neurons that may be altered by LFPI. **(A)** Excitatory synapses from LA, cortical, or thalamic afferents. **(B)** Excitatory synapses from LA, cortical, thalamic afferents (feedforward inhibition) or neighboring BLA pyramidal neurons (feedback inhibition). **(C)** Inhibitory synapses from local inhibitory interneurons onto a BLA pyramidal neuron.

Figures:

Figure 1

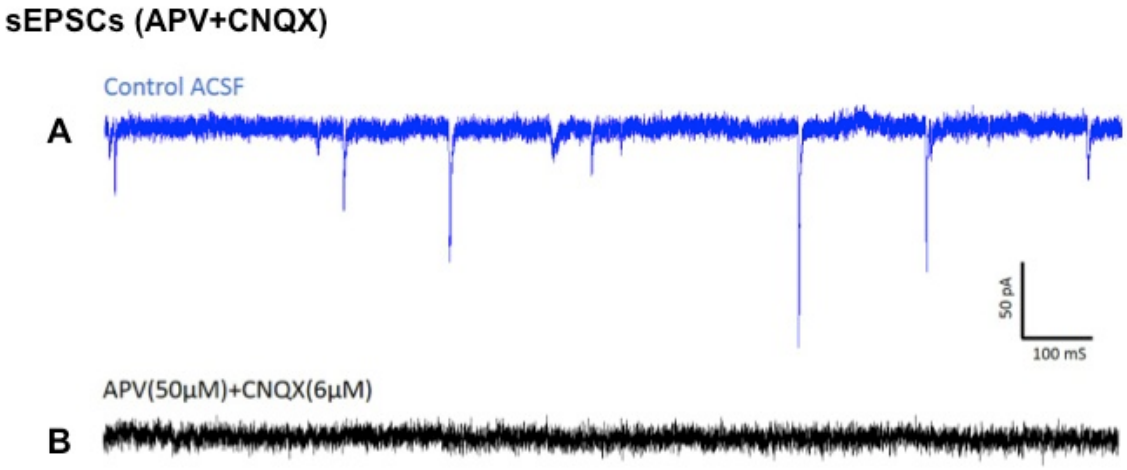

Figure 2

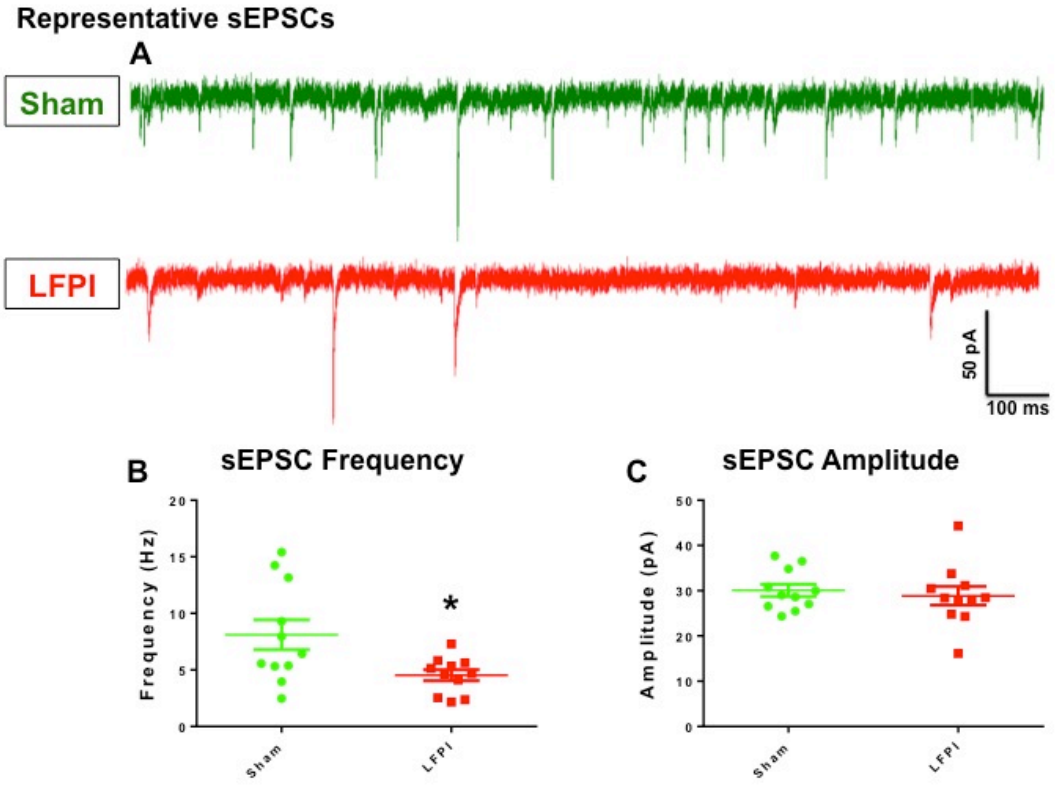
Representative sEPSCs
A
Sham
LFPI
50 pA
100 ms
B
sEPSC Frequency
Frequency (Hz)
20
15
10
5
0
*
Sham
LFPI
C
sEPSC Amplitude
Amplitude (pA)
50
40
30
20
10
0
Sham
LFPI

Figure 3

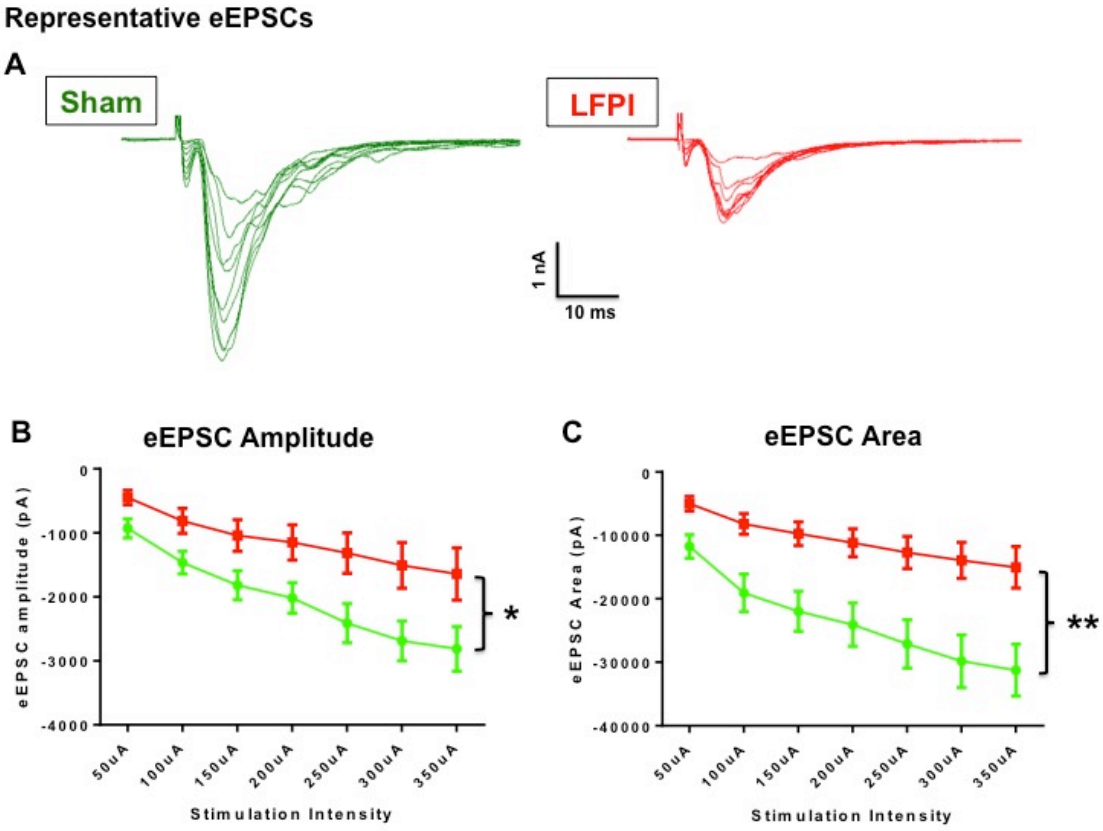
Representative eEPSCs
A
Sham
LFPI
1 nA
10 ms
B
eEPSC Amplitude
eEPSC amplitude (pA)
0
-1000
-2000
-3000
-4000
*
50uA
100uA
150uA
200uA
250uA
300uA
350uA
Stimulation Intensity
C
eEPSC Area
eEPSC Area (pA)
0
-10000
-20000
-30000
-40000
**
50uA
100uA
150uA
200uA
250uA
300uA
350uA
Stimulation Intensity

Figure 4

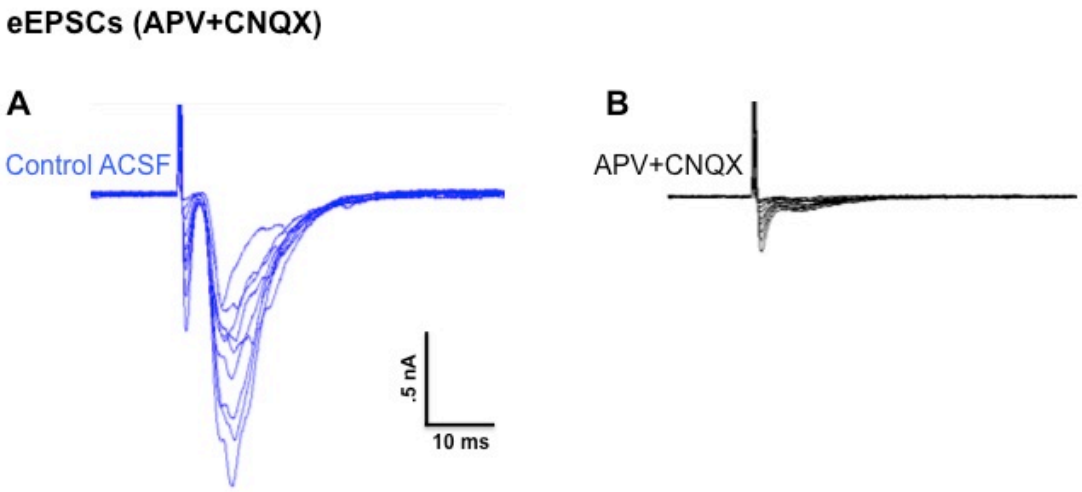

Figure 5

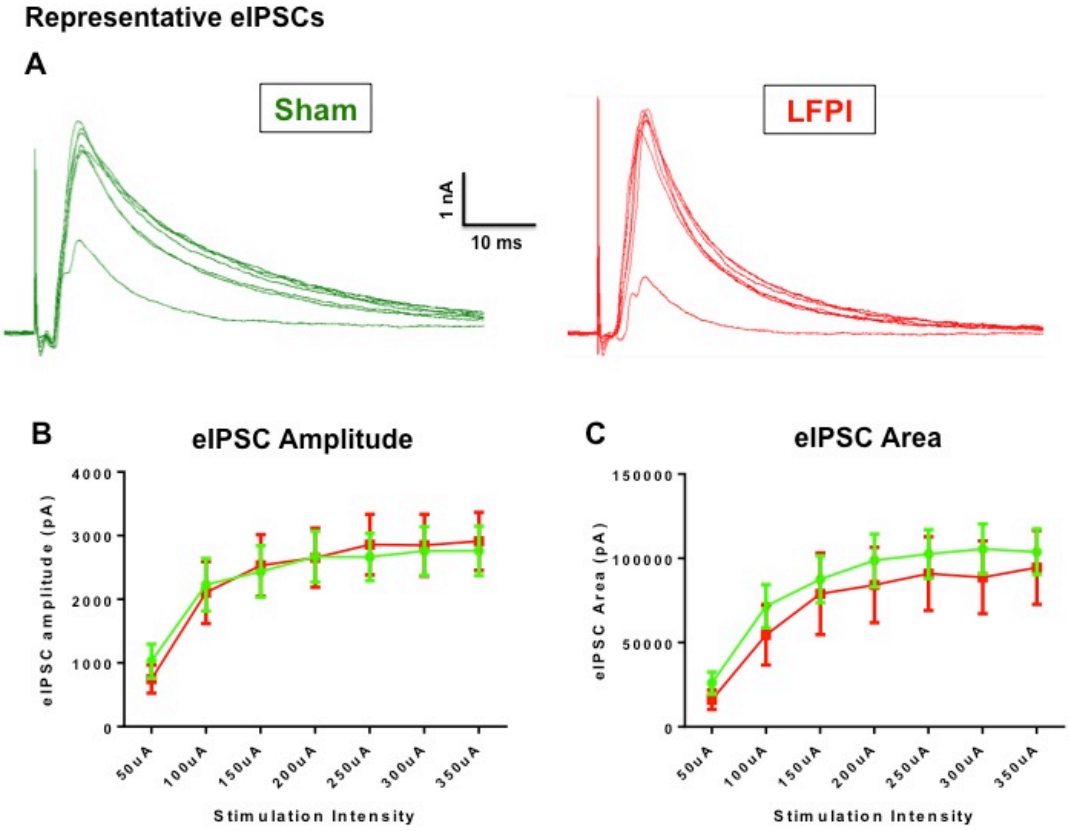
Representative eIPSCs
A
Sham
LFPI
1 nA
10 ms
B
eIPSC Amplitude
eIPSC amplitude (pA)
4000
3000
2000
1000
0
50uA
100uA
150uA
200uA
250uA
300uA
350uA
Stimulation Intensity
C
eIPSC Area
eIPSC Area (pA)
150000
100000
50000
0
50uA
100uA
150uA
200uA
250uA
300uA
350uA
Stimulation Intensity

Figure 6

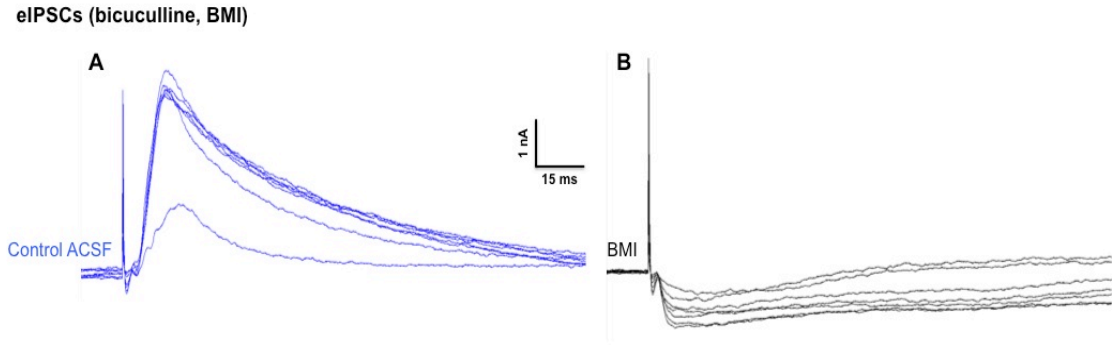

Figure 7

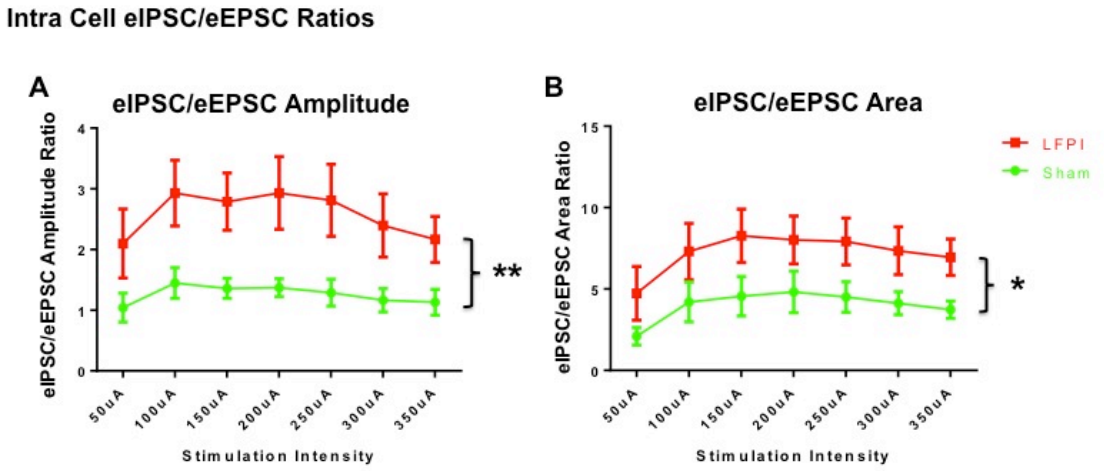
Intra Cell eIPSC/eEPSC Ratios
A
eIPSC/eEPSC Amplitude
eIPSC/eEPSC Amplitude Ratio
0
1
2
3
4
**
50uA
100uA
150uA
200uA
250uA
300uA
350uA
Stimulation Intensity
B
eIPSC/eEPSC Area
eIPSC/eEPSC Area Ratio
0
5
10
15
*
LFPI
Sham
50uA
100uA
150uA
200uA
250uA
300uA
350uA
Stimulation Intensity

Figure 8

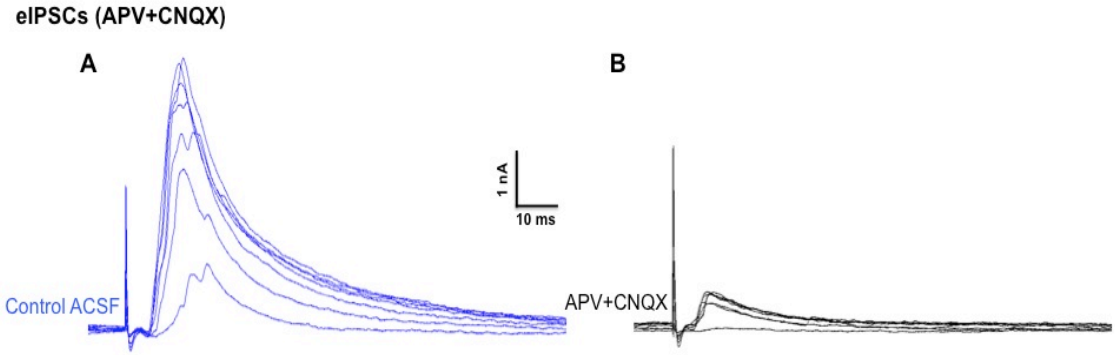

Figure 9

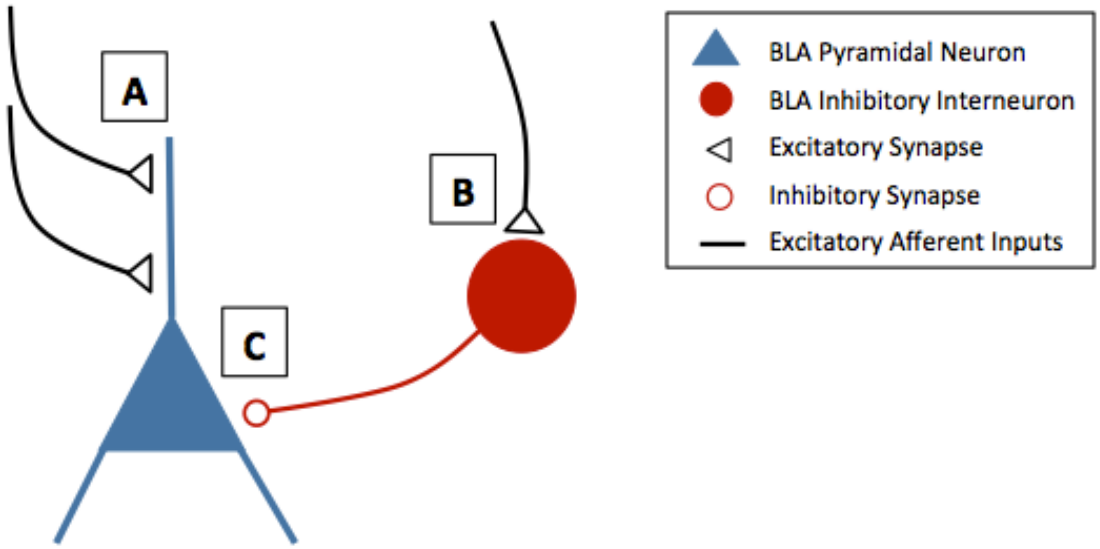
A
B
C
BLA Pyramidal Neuron
BLA Inhibitory Interneuron
Excitatory Synapse
Inhibitory Synapse
Excitatory Afferent Inputs

CHAPTER 4

Conclusions and Future Directions

Conclusions:

Choosing a focus of study as a scientist and academic is a bit like choosing the subject of a painting. We study things that captivate us, for motivations shared and our own. We all seek to learn and educate, better ourselves, and hope that in some small way we can enrich the lives and minds of others in the process. At the culmination of this particular study I digress to thinking of what motivated it in the first place. As much as we try to avoid it and take measures to prevent it, injury is a part of life, a natural consequence of the act of living. To me, an injury that can change the very essence of who we are, our personality, our emotions and our motivations is the most frightening, yet also the most intriguing. To that end, brain injury and its consequences, that can change the way we think and behave, are what I chose to study.

The overarching goal of the work presented in this thesis is to add to our limited understanding of physiological alterations in the brain that underlie the neuropsychological symptoms of traumatic brain injury (TBI). To accomplish this, we performed a series of behavioral and electrophysiological experiments assessing amygdalar function in animals that sustained a mild traumatic brain injury (mTBI). These experiments demonstrated that mTBI causes a substantial perturbation of amygdalar physiology, which alters the animal's perception of or reaction to, sensory stimuli.

The data presented in chapter 2 demonstrate a significant deficit in an amygdala-dependent behavior, behavioral threat response (a.k.a. cued fear conditioning), 7 days after lateral fluid percussion injury (LFPI). This behavioral deficit corresponded to significant decreases in network excitability and activation of the basolateral and central amygdalae (BLA & CeA). The overall decrease in excitability was due to a decrease in excitability of the primary input region of the amygdala, the lateral amygdala (LA) and a congruent decrease in signal propagation of activation through the amygdala circuit. Further experiments demonstrated that the intrinsic excitability and membrane properties of the principal cell type within the BLA are unaltered by LFPI. Together, the physiological data demonstrates that LFPI causes robust circuit level dysfunction in the amygdala without altering the intrinsic excitability of the principal excitatory cell type.

When conceptualizing the relation of behavioral phenomena in animals, such as behavioral threat response, to the subjective experience of human emotions or feelings, it is important to consider that these phenomena are distinct, yet unequivocally linked. While it is difficult to relate a behavioral threat response based on survival instinct and built upon survival circuitry directly to a subjective human emotion, these survival circuits and instincts that we study in animals are present in humans. Human survival instincts and circuits are perhaps more complex, but they doubtless contribute to the higher order emotional responses and subjective feelings humans experience (Phelps and LeDoux, 2005; LeDoux, 2012). See (LeDoux, 2012) for an in depth consideration of and current opinions on this topic.

Experiments discussed in Chapter 3 investigated the potential underlying mechanism of the injury-induced decrease in network excitability and circuit strength of the BLA. Results from these experiments demonstrate that LFPI causes a decrease in glutamatergic excitation onto BLA pyramidal neurons, with no change in the amount of GABAergic inhibition. As the vast majority of inhibition recorded under these conditions is feedforward/feedback inhibition, dependent upon activation by glutamatergic synapses; the lack of a decrease in inhibition corresponding to the significant decrease in excitation, suggests that LFPI also selectively augments or preserves polysynaptic inhibition in the BLA. Overall, the results of these experiments reveal opposing shifts in glutamatergic excitation and GABAergic inhibition, which increase the ratio of inhibition to excitation within the BLA following LFPI.

The research presented in Chapters 2 and 3 represent the most comprehensive examination of the effects of TBI on amygdala physiology performed to date. These experiments show that the amygdala can be and is affected in animal models of traumatic brain injury, even injury models with relatively distant focal points, like the LFPI model used here. Furthermore, the discovery that brain injury alters the ratio of synaptic excitation to inhibition in the amygdala, affords additional support to the hypothesis that TBI causes a disruption of E/I balance in the brain. An outcome that has now been observed in the hippocampus, medial prefrontal cortex and amygdala following TBI (Witgen et al., 2005; Smith et al., 2015; Palmer et al., 2016). Interestingly, the direction and nature of the shifts in E/I balance seem to be brain region specific, rather than a

global brain phenomenon. This is perhaps due to the unique complement of cell types and circuit organization in each brain region. Additionally, the results showing that polysynaptic feedforward/feedback inhibition is selectively augmented or preserved in the BLA of brain injured animals, suggests a potential cell type specific effect of TBI in the amygdala; though further experiments are required to confirm this observation and identify a potential cell type. Finally, this is the first study to identify reduced network excitability and circuit strength in the amygdala, acutely after TBI. As a decrease in amygdalar excitability is typically associated with decreases in anxiety like behaviors, this work also provides a heretofore-missing physiological substrate for the behavioral studies, discussed in the introduction, that describe a reduction or no change in anxiety like behaviors following TBI.

Future Directions:

The findings presented in the supplementary materials of Chapter 2, and the preliminary nature of Chapter 3, identify several potential future investigations that would directly build upon the data presented in those chapters. A more holistic consideration of the data presented in this thesis, within the context of human TBI, also identifies a number of interesting follow up studies that could expand upon the work herein. This research also opens avenues to a very translational line of experiments by providing a paradigm in which to test future therapeutics. Potential interventions could be targeted at mitigating or ameliorating mTBI-induced amygdala dysfunction, for the treatment of the neuropsychological symptoms associated with TBI.

While the physiological findings presented in Chapter 2 correspond to alterations in an amygdala dependent behavior, it would be very interesting to correlate our physiological results with the results of additional behavioral experiments assessing anxiety, depression and aggression like behaviors. To accomplish this we would employ our existing injury model, then compare the results of sham and LFPI animals in the elevated plus/zero maze/open field (anxiety), tail suspension/forced swim (depression), and resident intruder (aggression) behavioral paradigms. These paradigms would likely require separate cohorts of animals, as the amygdala is extremely sensitive to the stress induced by these experiments, such that the stress of one experiment could alter the findings of another. These experiments would help to identify which, if any, of the neuropsychological symptoms of TBI correlate with the observed amygdala physiological deficits. This in turn could help identify human patients, based on the symptoms they present, who may benefit from a therapy that mitigates amygdala deficits in this animal model. It would also be important to perform these experiments at more prolonged post-injury time points, as discussed later in this chapter, to assess these behaviors at time points which better correlate to the development of human neuropsychological symptoms.

In Chapter 2 the slow negative-going peak (SNP) of the VSD signal was significantly more hyperpolarized in the amygdalae of brain slices from LFPI animals (Chapter 2, Fig 3). Given that the SNP is mediated by $GABA_B$ receptors (Chapter 2, Fig. S3), the increase in SNP hyperpolarization in LFPI slices could represent an injury induced-increase in $GABA_B$ signaling. Alternatively, this difference in the SNP could

simply be the result of a decrease in glial depolarization corresponding with the observed decease in neuronal depolarization, as glia likely mediate the opposing depolarization present at the time of the SNP. To isolate and measure the $GABA_B$ mediated signal, we would apply a $GABA_B$ antagonist (CGP55845) and calculate the difference in pre vs. post drug SNP $\Delta F/F$, as the magnitude of the $GABA_B$ signal in brain slices from sham and LFPI animals. Such a study would determine if LFPI augments $GABA_B$ signaling in the amygdala.

The experiments discussed in Chapter 3 are the beginnings of a larger study that will seek to confirm and identify the source of augmented feedforward/feedback inhibition in the BLA following LFPI. The next logical experiment would be to record spontaneous inhibitory post synaptic currents (sIPSCs) onto BLA pyramidal neurons. This experiment could help identify if the alteration in inhibition is likely due to a presynaptic or postsynaptic mechanism (see Chapter 3 discussion for hypotheses). If these experiments suggest a presynaptic mechanism, it's plausible that the augmented inhibition is due to an increase in output of a particular type of inhibitory interneuron, as has been previously demonstrated in the hippocampus (Johnson et al., 2014). Pharmacological or optogenetic manipulations could be employed to search for the cell type mediating this increase in inhibition. As the BLA contains CCK+ interneurons similar to the CCK+ interneurons that contribute to augmented inhibition in area CA1 of the hippocampus following LFPI (Johnson et al., 2014); assessing the function of these neurons in the BLA would be the logical place to begin.

When taking a broader view of the work presented in this thesis and comparing it to human TBI research, it is evident that the time point after injury when these experiments were performed, may be an important parameter to consider. Given the sub-acute window in which human TBI patients develop neuropsychological issues, it's possible that the acute (7 days after injury) physiological alterations in the amygdala, characterized in this study, don't correlate to any human neuropsychological symptoms; which typically develop months or even years after TBI. Rather, this acute physiological dysfunction may represent a consequence of the initial insult, which primes overcompensation or an imperfect homeostatic response, to the acute decrease in amygdala network excitability. It's conceivable that overcompensation could even lead to an overall increase in network excitability in the amygdala at later time points.

Injury-induced alterations to amygdalar physiology are likely a dynamic process that will change and perhaps even recover over time. Future experiments assessing amygdala physiology and behaviors at more prolonged time points after injury, would allow us to characterize the progression of amygdala dysfunction and examine amygdala physiology at a post injury time point that correlates with the development of human neuropsychological symptoms. This could be accomplished by replicating the experiments discussed in Chapter 2 at 14, 30 and 60 days post-LFPI. The results of these experiments could lead to a more in depth characterization of the progression of injury-induced physiological dysfunction in the amygdala, and further inform our interpretation of the data presented in Chapters 2 & 3 of this thesis.

Previous work from our laboratory has demonstrated that administration of high concentration branched chain amino acids (BCAAs) acutely after injury, can prevent or ameliorate injury-induced physiological dysfunction of the hippocampus and the resulting cognitive deficits (Cole et al., 2010; Elkind et al., 2015). This work has led to an ongoing clinical trial assessing the efficacy of BCAAs to improve neurocognitive recovery in human mTBI patients. As previously discussed, injury-induced physiological alterations in the amygdala are the result of a disruption of E/I balance, similar to the disruption of E/I balance seen in area CA1 of the hippocampus. Given the similarity of injury effects in these brain regions, it is certainly possible that BCAA administration could ameliorate amygdala dysfunction following TBI. To assess the efficacy of BCAAs in restoring normal amygdala function, we would again replicate the experiments discussed in Chapter 2 in a cohort of brain injured animals treated with high concentration BCAAs. If BCAAs successfully restore normal amygdala physiology and function, this would suggest that BCAAs might be effective in the treatment or prevention of neuropsychological symptoms following TBI.

Translating the results of murine research to a human condition and proving those results are relevant to the human condition, is difficult at best. It often involves a great many assumptions and years of replicating experiments in higher order mammals. However, the lack of adverse events associated with administration of high concentration BCAAs to humans, and the absence of any alternative treatment for mTBI; make for a unique situation, where the results of the suggested murine experiments could be directly tested in a human patient population. The positive results of BCAAs in our TBI animal

model have already prompted a human clinical trial focused on neurocognitive recovery. If further research indicates that BCAAs prevent amygdala dysfunction, this could prompt another human trial assessing the efficacy of BCAAs to prevent or mitigate the development of neuropsychological symptoms following TBI. The possibility that this work could so quickly be tested in a human patient population emphasizes the translational nature and value of such studies.

BIBLIOGRAPHY

Ajao DO, Pop V, Kamper JE, Adami A, Rudobeck E, Huang L, Vlkolinsky R, Hartman RE, Ashwal S, Obenaus A, Badaut J (2012) Traumatic brain injury in young rats leads to progressive behavioral deficits coincident with altered tissue properties in adulthood. Journal of Neurotrauma 29:2060–2074.

Almeida-Suhett CP, Prager EM, Pidoplichko V, Figueiredo TH, Marini AM, Li Z, Eiden LE, Braga MFM (2014) Reduced GABAergic Inhibition in the Basolateral Amygdala and the Development of Anxiety-Like Behaviors after Mild Traumatic Brain Injury Rudolph U, ed. PLoS ONE 9:e102627.

Alves W, Macciocchi SN, Barth JT (1993) Postconcussive symptoms after uncomplicated mild head injury. J Head Trauma Rehabil.

Ang CW, Carlson GC, Coulter DA (2006) Massive and Specific Dysregulation of Direct Cortical Input to the Hippocampus in Temporal Lobe Epilepsy. Journal of Neuroscience 26:11850–11856.

Avrabos C, Sotnikov SV, Dine J, Markt PO, Holsboer F, Landgraf R, Eder M (2013) Real-Time Imaging of Amygdalar Network Dynamics In Vitro Reveals a Neurophysiological Link to Behavior in a Mouse Model of Extremes in Trait Anxiety. Journal of Neuroscience 33:16262–16267.

Bazarian JJ, Cernak I, Noble-Haeusslein L, Potolicchio S, Temkin N (2009) Long-term neurologic outcomes after traumatic brain injury. J Head Trauma Rehabil 24:439–

451.

Benedictus MR, Spikman JM, van der Naalt J (2010) Cognitive and Behavioral Impairment in Traumatic Brain Injury Related to Outcome and Return to Work. Archives of Physical Medicine and Rehabilitation 91:1436–1441.

Blennow K, Hardy J, Zetterberg H (2012) The Neuropathology and Neurobiology of Traumatic Brain Injury. Neuron 76:886–899.

Blume H, Hawash K (2012) Subacute concussion-related symptoms and postconcussion syndrome in pediatrics. Current Opinion in Pediatrics 24:724–730.

Bourgeois EB, Johnson BN, McCoy AJ, Trippa L, Cohen AS, Marsh ED (2014) A Toolbox for Spatiotemporal Analysis of Voltage-Sensitive Dye Imaging Data in Brain Slices Dravid SM, ed. PLoS ONE 9:e108686.

Budinich CS, Tucker LB, Lowe D, Rosenberger JG, McCabe JT (2013) Pharmacology, Biochemistry and Behavior. Pharmacol Biochem Behav 108:66–73.

Carbonell WS, Maris DO, McCall T, Grady MS (1998) Adaptation of the fluid percussion injury model to the mouse. Journal of Neurotrauma 15:217–229.

Cardinal RN, Parkinson JA, Hall J, Everitt BJ (2002) Emotion and motivation: the role of the amygdala, ventral striatum, and prefrontal cortex. Neurosci Biobehav Rev 26:321–352.

Carlson GC, Coulter DA (2008) In vitro functional imaging in brain slices using fast

voltage-sensitive dye imaging combined with whole-cell patch recording. Nat Protoc 3:249–255.

Chen Y, Mao H, Yang KH, Abel T, Meaney DF (2014) A modified controlled cortical impact technique to model mild traumatic brain injury mechanics in mice. Front Neur 5:100.

Cole JT, Mitala CM, Kundu S, Verma A, Elkind JA, Nissim I, Cohen AS (2010) Dietary branched chain amino acids ameliorate injury-induced cognitive impairment. Proceedings of the National Academy of Sciences 107:366–371.

Cutler SM, VanLandingham JW, Murphy AZ, Stein DG (2006) Slow-release and injected progesterone treatments enhance acute recovery after traumatic brain injury. Pharmacol Biochem Behav 84:420–428.

D RCWHM, D RCWHM, Chapman MJ (2011) Definition, diagnosis, and forensic implications of postconcussional syndrome. Psychosomatics 46:195–202.

Depue BE, Olson-Madden JH, Smolker HR, Rajamani M, Brenner LA, Banich MT (2014) Reduced Amygdala Volume Is Associated with Deficits in Inhibitory Control: A Voxel- and Surface-Based Morphometric Analysis of Comorbid PTSD/Mild TBI. BioMed Research International 2014:1–11.

Dębiec J, Díaz-Mataix L, Bush DEA, Doyère V, LeDoux JE (2010) The amygdala encodesspecific sensory featuresof an aversive reinforcer. Nature Publishing Group 13:536–537.

Dockree PM, Robertson IH (2011) Electrophysiological markers of cognitive deficits in Traumatic Brain Injury: A review. International Journal of Psychophysiology 82:53–60 Available at: http://linkinghub.elsevier.com/retrieve/pii/S0167876011000055.

Duncan CC, Kosmidis MH, Mirsky AF (2003) Event-related potential assessment of information processing after closed head injury. Psychophysiology 40:45–59.

Duvarci S, Pare D (2014) Amygdala Microcircuits Controlling Learned Fear. Neuron 82:966–980.

Ehrlich I, Humeau Y, Grenier F, Ciocchi S, Herry C, Lüthi A (2009) Amygdala Inhibitory Circuits and the Control of Fear Memory. Neuron 62:757–771.

Elkind JA, Lim MM, Johnson BN, Palmer CP, Putnam BJ, Kirschen MP, Cohen AS (2015) Efficacy, dosage, and duration of action of branched chain amino Acid therapy for traumatic brain injury. Front Neur 6:73.

Faul F, Erdfelder E, Lang A-G, Buchner A (2007) G*Power 3: a flexible statistical power analysis program for the social, behavioral, and biomedical sciences. Behav Res Methods 39:175–191.

Faul M, Coronado V (2015) Epidemiology of traumatic brain injury. Handb Clin Neurol 127:3–13.

Finkelstein EA, Corso PS, Miller TR (2006) Incidence and Economic Burden of Injuries in the United States - Public Health Economics Program Eric A. Finkelstein Senior Health Economist, Division for Health Services and Social Policy Research Research

Triangle International, National Center for Injury Prevention and Control Centers for Disease Control and Prevention Phaedra S. Corso Senior Health Economist, Calverton Ted R. Miller Principal Research Scientist and Site Director Pacific Institute for Research and Evaluation, Maryland - Google Books.

Fredj NB, Burrone J (2009) A resting pool of vesicles is responsible for spontaneous vesicle fusion at the synapse. Nat Neurosci 12:751–758.

Gupta A, Elgammal FS, Proddutur A, Shah S, Santhakumar V (2012) Decrease in Tonic Inhibition Contributes to Increase in Dentate Semilunar Granule Cell Excitability after Brain Injury. Journal of Neuroscience 32:2523–2537.

Han K, Chapman SB, Krawczyk DC (2015) Altered Amygdala Connectivity in Individuals with Chronic Traumatic Brain Injury and Comorbid Depressive Symptoms. Front Neur 6:36.

Johansson B, Berglund P, Rönnbäck L (2009) Mental fatigue and impaired information processing after mild and moderate traumatic brain injury. Brain Inj 23:1027–1040.

Johnson B, Zhang K, Gay M, Horovitz S, Hallett M, Sebastianelli W, Slobounov S (2012) Alteration of brain default network in subacute phase of injury in concussed individuals: Resting-state fMRI study. NeuroImage 59:511–518.

Johnson BN, Palmer CP, Bourgeois EB, Elkind JA, Putnam BJ, Cohen AS (2014) Augmented Inhibition from Cannabinoid-Sensitive Interneurons Diminishes CA1 Output after Traumatic Brain Injury. Front Cell Neurosci 8:435.

Jones NC, Cardamone L, Williams JP, Salzberg MR, Myers D, O'Brien TJ (2008) Experimental Traumatic Brain Injury Induces a Pervasive Hyperanxious Phenotype in Rats. Journal of Neurotrauma 25:1367–1374.

Jorge RE, Robinson RG, Moser D, Tateno A, Crespo-Facorro B, Arndt S (2004) Major depression following traumatic brain injury. Arch Gen Psychiatry 61:42–50.

Juranek J, Johnson CP, Prasad MR, Kramer LA, Saunders A, Filipek PA, Swank PR, Cox CS, Ewing-Cobbs L (2011) Mean diffusivity in the amygdala correlates with anxiety in pediatric TBI. Brain Imaging and Behavior 6:36–48.

Kimbler DE, Shields J, Yanasak N, Vender JR, Dhandapani KM (2012) Activation of P2X7 Promotes Cerebral Edema and Neurological Injury after Traumatic Brain Injury in Mice Kleinschnitz C, ed. PLoS ONE 7:e41229.

Klein RC, Acheson SK, Qadri LH, Dawson AA, Rodriguiz RM, Wetsel WC, Moore SD, Laskowitz DT, Dawson HN (2015) Opposing effects of traumatic brain injury on excitatory synaptic function in the lateral amygdala in the absence and presence of preinjury stress. J Neurosci Res:n/a–n/a.

Langlois JA, Rutland-Brown W, Wald MM (2006) The epidemiology and impact of traumatic brain injury: a brief overview. J Head Trauma Rehabil 21:375–378.

LeDoux J (2012) Perspective. Neuron 73:653–676.

Ledoux JE (2000) Emotion circuits in the brain. Annu Rev Neurosci 23:155–184.

Leung LS, Zhao D (1995) Glial potentials evoked by single afferent pulses in hippocampal CA1 area in vitro. Brain Research 697:262–265.

Liao C, Feng Z, Zhou D, Dai Q, Xie B, Ji B, Wang X, Wang X (2012) DYSFUNCTION OF FRONTO-LIMBIC BRAIN CIRCUITRY IN DEPRESSION. NSC 201:231–238.

Malkesman O, Tucker LB, Ozl J, McCabe JT (2013) Traumatic brain injury - modeling neuropsychiatric symptoms in rodents. Front Neur 4:157.

Mayer AR, Mannell MV, Ling J, Gasparovic C, Yeo RA (2011) Functional connectivity in mild traumatic brain injury. Hum Brain Mapp 32:1825–1835.

McAllister TW (1992) Neuropsychiatric sequelae of head injuries. Psychiatric Clinics of North America.

McAllister TW, Flashman LA, McDonald BC, Saykin AJ (2006) Mechanisms of working memory dysfunction after mild and moderate TBI: evidence from functional MRI and neurogenetics. Journal of Neurotrauma 23:1450–1467.

Milman A, Rosenberg A, Weizman R, Pick CG (2005) Mild traumatic brain injury induces persistent cognitive deficits and behavioral disturbances in mice. Journal of Neurotrauma 22:1003–1010.

Newton JR, Ellsworth C, Miyakawa T, Tonegawa S, Sur M (2004) Acceleration of visually cued conditioned fear through the auditory pathway. Nat Neurosci 7:968–973.

Palmer CP, Metheny HE, Elkind JA, Cohen AS (2016) Diminished amygdala activation and behavioral threat response following traumatic brain injury. Experimental Neurology 277:215–226.

Pandey DK, Yadav SK, Mahesh R, Rajkumar R (2009) Depression-like and anxiety-like behavioural aftermaths of impact accelerated traumatic brain injury in rats: a model of comorbid depression and anxiety? Behavioural Brain Research 205:436–442.

Phelps EA, LeDoux JE (2005) Contributions of the Amygdala to Emotion Processing: From Animal Models to Human Behavior. Neuron 48:175–187.

Phillips RG, Ledoux JE (1992) Differential contribution of amygdala and hippocampus to cued and contextual fear conditioning. Behavioral Neuroscience 106:274–285.

Prager EM, Bergstrom HC, Wynn GH, Braga MFM (2015) The basolateral amygdala γ-aminobutyric acidergic system in health and disease. J Neurosci Res:n/a–n/a.

Rainnie DG, Asprodini EK, Shinnick-Gallagher P (1991) Inhibitory transmission in the basolateral amygdala. Journal of Neurophysiology 66:999–1009.

Rao V, Rosenberg P, Bertrand M, Salehinia S, Spiro J, Vaishnavi S, Rastogi P, Noll K, Schretlen DJ, Brandt J, Cornwell E, Makley M, Miles QS (2009) Aggression after traumatic brain injury: prevalence and correlates. J Neuropsychiatry Clin Neurosci 21:420–429.

Reger ML, Poulos AM, Buen F, Giza CC, Hovda DA, Fanselow MS (2012) Concussive Brain Injury Enhances Fear Learning and Excitatory Processes in the Amygdala.

Biological Psychiatry 71:335–343.

Riggio S (2010) Traumatic Brain Injury and Its Neurobehavioral Sequelae. Psychiatric Clinics of North America 33:807–819.

Rutland-Brown W, Langlois JA, Thomas KE, Xi YL (2006) Incidence of traumatic brain injury in the United States, 2003. J Head Trauma Rehabil 21:544.

Sah P, Faber ESL, Lopez De Armentia M, Power J (2003) The amygdaloid complex: anatomy and physiology. Physiol Rev 83:803–834.

Santhakumar V, Ratzliff ADH, Jeng J, Toth Z, Soltesz I (2002) Long-term hyperexcitability in the hippocampus after experimental head trauma. Ann Neurol 50:708–717.

Sánchez-Carrión R, Gómez PV, Junqué C, Fernández-Espejo D, Falcon C, Bargalló N, Roig-Rovira T, Enseñat-Cantallops A, Bernabeu M (2008) Frontal Hypoactivation on Functional Magnetic Resonance Imaging in Working Memory after Severe Diffuse Traumatic Brain Injury. Journal of Neurotrauma 25:479–494.

Scholten AC, Haagsma JA, Cnossen MC, Olff M, Van Beeck EF, Polinder S (2016) Prevalence and risk factors of anxiety and depressive disorders following traumatic brain injury: a systematic review. Journal of Neurotrauma:neu.2015.4252.

Schwarzbold ML, Rial D, De Bem T, Machado DG, Cunha MP, Santos dos AA, Santos dos DB, Figueiredo CP, Farina M, Goldfeder EM, Rodrigues ALS, Prediger RDS, Walz R (2010) Effects of Traumatic Brain Injury of Different Severities on

Emotional, Cognitive, and Oxidative Stress-Related Parameters in Mice. Journal of Neurotrauma 27:1883–1893.

Semple BD, Canchola SA, Noble-Haeusslein LJ (2012) Deficits in Social Behavior Emerge during Development after Pediatric Traumatic Brain Injury in Mice. Journal of Neurotrauma 29:2672–2683.

Sharp DJ, Scott G, Leech R (2014) Network dysfunction after traumatic brain injury. Nature Publishing Group 10:156–166.

Shultz SR, Bao F, Omana V, Chiu C, Brown A, Cain DP (2012) Repeated mild lateral fluid percussion brain injury in the rat causes cumulative long-term behavioral impairments, neuroinflammation, and cortical loss in an animal model of repeated concussion. Journal of Neurotrauma 29:281–294.

Siopi E, Llufriu-Dabén G, Fanucchi F, Plotkine M, Marchand-Leroux C, Jafarian-Tehrani M (2012) Evaluation of late cognitive impairment and anxiety states following traumatic brain injury in mice: the effect of minocycline. Neuroscience Letters 511:110–115.

Slovarp L, Azuma T, LaPointe L (2012) The effect of traumatic brain injury on sustained attention and working memory. Brain Inj 26:48–57.

Smith CJ, Xiong G, Elkind JA, Putnam B, Cohen AS (2015) Brain Injury Impairs Working Memory and Prefrontal Circuit Function. Front Neur 6:1.

Tateno A, Jorge RE, Robinson RG (2003) Clinical correlates of aggressive behavior after

traumatic brain injury. J Neuropsychiatry Clin Neurosci 15:155–160.

Taylor AN, Rahman SU, Tio DL, Sanders MJ, Bando JK, Truong AH, Prolo P (2006) Lasting neuroendocrine-immune effects of traumatic brain injury in rats. Journal of Neurotrauma 23:1802–1813.

Thompson HJ, Lifshitz J, Marklund N, Grady MS, Graham DI, Hovda DA, McIntosh TK (2005) Lateral fluid percussion brain injury: a 15-year review and evaluation. Journal of Neurotrauma 22:42–75.

Tominaga T, Tominaga Y, Yamada H, Matsumoto G, Ichikawa M (2000) Quantification of optical signals with electrophysiological signals in neural activities of Di-4-ANEPPS stained rat hippocampal slices. Journal of Neuroscience Methods 102:11–23.

Tran LD, Lifshitz J, Witgen BM, Schwarzbach E, Cohen AS, Grady MS (2006) Response of the contralateral hippocampus to lateral fluid percussion brain injury. Journal of Neurotrauma 23:1330–1342.

Tronson NC, Corcoran KA, Jovasevic V, Radulovic J (2012) Fear conditioning and extinction: emotional states encoded by distinct signaling pathways. Trends in Neurosciences 35:145–155.

Tweedie D, Milman A, Holloway HW, Li Y, Harvey BK, Shen H, Pistell PJ, Lahiri DK, Hoffer BJ, Wang Y, Pick CG, Greig NH (2007) Apoptotic and behavioral sequelae of mild brain trauma in mice. J Neurosci Res 85:805–815.

Vučković MG, Wood RI, Holschneider DP, Abernathy A, Togasaki DM, Smith A, Petzinger GM, Jakowec MW (2008) Neurobiology of Disease. Neurobiol Dis 32:319–327.

Wagner AK, Kline AE, Ren D, Willard LA, Wenger MK, Zafonte RD, Dixon CE (2007) Gender associations with chronic methylphenidate treatment and behavioral performance following experimental traumatic brain injury. Behavioural Brain Research 181:200–209.

Washington PM, Forcelli PA, Wilkins T, Zapple DN, Parsadanian M, Burns MP (2012) The effect of injury severity on behavior: a phenotypic study of cognitive and emotional deficits after mild, moderate, and severe controlled cortical impact injury in mice. Journal of Neurotrauma 29:2283–2296.

Witgen BM, Lifshitz J, Smith ML, Schwarzbach E, Liang SL, Grady MS, Cohen AS (2005) Regional hippocampal alteration associated with cognitive deficit following experimental brain injury: A systems, network and cellular evaluation. Neuroscience 133:1–15.

Wolff SBE, Gründemann J, Tovote P, Krabbe S, Jacobson GA, Müller C, Herry C, Ehrlich I, Friedrich RW, Letzkus JJ, Lüthi A (2014) Amygdala interneuron subtypes control fear learning through disinhibition. Nature 509:453–458.

Wong JC, Linn KA, Shinohara RT, Mateen FJ (2015) Traumatic brain injury in Africa in 2050: a modeling study. Eur J Neurol 23:382–386.

Xiong Y, Mahmood A, Chopp M (2013) Animal models of traumatic brain injury. Nat Rev Neurosci 14:128–142.

Yamada J, Saitow F, Satake S, Kiyohara T, Konishi S (1999) GABA(B) receptor-mediated presynaptic inhibition of glutamatergic and GABAergic transmission in the basolateral amygdala. Neuropharmacology 38:1743–1753.

Yu F, Wang Z, Tchantchou F, Chiu C-T, Zhang Y, Chuang D-M (2012) Lithium Ameliorates Neurodegeneration, Suppresses Neuroinflammation, and Improves Behavioral Performance in a Mouse Model of Traumatic Brain Injury. Journal of Neurotrauma 29:362–374.

Zaloshnja E, Miller T, Langlois JA, Selassie AW (2008) Prevalence of long-term disability from traumatic brain injury in the civilian population of the United States, 2005. J Head Trauma Rehabil 23:394–400.